"Model Testing on the Offshore Event Effects"
Project # 187 (U. Houston), June 1994

ABSTRACT

During earthquakes pore water pressure is generated around piles in offshore structures. This increase in the pore water pressure causes a decrease in the effective confining stresses around piles and thus causes a degradation in the soil strength.

A method is presented to degrade the t-z curves in a tension-loaded pile subjected to earthquake type loading. This method uses effective stress analysis to model the effect of pore water pressure buildup during the seismic event.

A degradation factor (ρ) which depends upon the pore water pressure increase is used to degrade both the p-y curves and t-z curves. This degradation factor is reevaluated according to test results of a tension-loaded pile subjected to simulated seismic motion (Ochoa, 1990).

It was found that the degradation in the t-z curves is more severe than those predicted for the p-y curves.

Notations :

D	Pile diameter;
F	Factor that depends on the shape of the loaded area; typically ranges from 2-3;
G_{max}	Soil shear modulus at very low strain;
p	Lateral soil reaction on unit pile length;
r	Pore water pressure ratio $= \Delta u/\sigma'_{vo}$;
t	Vertical soil reaction on unit pile length;
y	Pile displacement in the lateral direction;
z	Pile displacement in the vertical direction;
Δu	Pore water pressure generated during the seismic event;
δ_1	Soil-pile spring coefficient that depends on the loading conditions; typically ranges from 1.20-1.75;
ϕ	Angle of internal friction of the soil;
γ	Shear strain, which is a function of the pile displacement (y);
γ_r	Reference strain; $= \tau_{max}/G_{max}$;
ν	Poisson's ratio of the soil;
ρ	Degradation factor which is the degraded soil reaction divided by the static reaction $= P_{dy}/P_{st}$;
σ_c	Effective isotropic confining pressure;
σ'_{vo}	Initial effective vertical stress;
σ'_v	Effective vertical stress; and
τ_{max}	Maximum shear stress $= \sin\phi\ \sigma'_{vo}/(1 - \sin\phi)$.

CHAPTER (1)

INTRODUCTION

CHAPTER (1)

INTRODUCTION

Response of pile supported structures during earthquakes may vary from catastrophic failure to a slight degradation in strength or even an increase in strength due to loading rate effects.

Offshore structures are usually supported on marine deposits which are usually softer than onshore soils, therefore; the effect of the earthquake on offshore piles is potentially more severe. The behavior of piles supporting offshore structures during earthquakes is affected by many variables including: earthquake magnitude, fault distance from the structure, soil characteristics, load on the pile, pile stiffness relative to the soil, pile spacing (if the pile is in a group) and many other factors.

During earthquake shaking, cohesionless soils tend to densify, causing an increase in the pore water pressure and a corresponding decrease in effective stress. This increase in the pore water pressure may cause a slight decrease in soil strength or may be high enough to cause liquefaction. Around a pile, the problem is more complex due to the fact that pile-soil interaction creates additional pore water pressure added to that originally generated in the free filed, and the presence of the pile also creates a change in the initial soil stresses and densities near the pile.

Degradation in soil strength around piles has been modeled by several investigators for both vertical and horizontal vibrations. Some research concentrated on the effect of earthquake type loading only, while others studied the problem under slower cyclic loading conditions.

Knowing that the strongest earthquake component is the horizontal one, many models have been proposed to degrade the lateral soil strength due to earthquake type loading (Matlock et al., 1978; Finn and Martin, 1979; Kagawa and Kraft, 1980a, b).

Effective stress models

Effective Stress Models to Degrade the p-y curves :

Finn and Martin (1979) proposed that the API p-y curves are to be degraded as a function of the generated pore water pressure during the earthquake in the free field as follows :

i) For small deflections in the elastic range, the initial soil modulus is assumed proportional to $(\sigma'_v)^{1/2}$. That is, the initial soil modulus defining the slope of the p-y curve at the origin is reduced by a factor $\{(\sigma'_{vo} - \Delta u)/\sigma'_{vo}\}^{1/2}$ where σ'_{vo} is the initial vertical effective stress, and Δu is the pore water pressure increase at time t;

ii) For deflections in the yielding range, soil strength characteristics dominate lateral resistance, and the p-y curve is degraded in proportion to σ'_v, that is, the p value is reduced by a factor $(\sigma'_{vo} - \Delta u)/\sigma'_{vo}$ if significant pore pressure dissipation can occur. If the loading is essentially undrained (as in our case study), recent laboratory data from undrained cyclic loading tests indicate that the strength degrades as $(\sigma'_v)^{1/2}$;

iii) The p-y curves between these two regions is drawn as described in the 1979 API procedure (Finn and Martin, 1979).

Alternatively, p-y curves can be modified for pore pressure buildup effects by reducing the p values on the static API curve by $(1 - r)^{1/2}$,

In which :

r is the pore water pressure ratio
$= \Delta u/\sigma'_{vo}$;

σ'_v is the effective vertical stress;

σ'_{vo} is the initial effective vertical stress; and

Δu is the induced excess pore water pressure during the seismic event.

Kagawa and Kraft, (1981c) developed a nonlinear cyclic p-y curve based on an effective stress model. This curve is described as follows:

$p = (1 - r)^{1/2} [2 F D \delta_1 G_{max} (\gamma/(1 + \gamma/\gamma_r))]$

In which :

p	is the soil reaction on unit pile length;
r	is the pore water pressure ratio $= \Delta u/\sigma'_{vo}$;
Δu	is the pore water pressure generated during the seismic event;
σ'_{vo}	is the initial effective vertical stress;
F	is a dimensionless factor that depends on the shape of the loaded area; typically ranges from 2-3;
D	is the pile diameter;
G_{max}	is the soil shear modulus at very low strain;
δ_1	is a dimensionless soil-pile spring coefficient that depends on the loading conditions typically ranges from 1.20-1.75;
γ	is the soil shear strain, which is a function of the pile displacement (y) $= (1 + \nu)y/FD$;
ν	is the Poisson's ratio of the soil;
y	is the pile displacement;
γ_r	is the reference strain $= \tau_{max}/G_{max}$;
τ_{max}	is the maximum shear stress $= \sin\phi\sigma'_{vo}/(1 - \sin\phi)$.

According to Kagawa and Kraft, (1981c), omitting the term $(1 - r)^{1/2}$ in their proposed cyclic p-y curve will reproduce the static API curve with an acceptable accuracy. However, their static curve was significantly lower than the curves given by the old and recent API p-y criteria, especially at large deflections (given in Appendix B). Nevertheless, they ascertain that the value $(1 - r)^{1/2}$ is a degradation factor for converting from static strength to cyclic strength.

Since the horizontal component of most earthquakes is the strongest, most previous research has focused only on the soil resistance degradation for lateral pile loading. However, the axial resistance is also degraded by the same pore water pressures in the soil mass that degrade the lateral resistance and additionally to potentially higher pore water pressure that can develop at the pile-soil interface due to cyclic vertical pile motion. The interface pore water pressure is the most important value for analysis of axially loaded pile capacity, whereas the soil mass pore water pressure, considered by the two studies referenced here, are more important for lateral loading. This concept leads to the following practical approach for using the results of model studies (Ochoa, 1990), to predict the uplift behavior of prototype cyclically loaded tension piles. This leads us to the assumptions in this work:

1- The degradation in the p-y curves is due to the pore water pressure buildup during the seismic event.
2- The degradation in the t-z curves (unit axial load-deformation curves) is equal to the degradation in the p-y curves, but this assumption will be reevaluated according to the results obtained form Phase II, Oceanside event tests (Ochoa, 1990).
3- Ochoa's model accurately represents the prototype pile, soil, and loading conditions (Ochoa, 1990).
4- Loading rate effects are not significant.
5- Pile tip suction during the cyclic loading does not have a significant effect in the pullout capacity of the pile.

Laboratory Model Tests:

Before proceeding to the method of analysis, the Phase II, Oceanside event model is described first. The model is 1 in. diameter steel tube, representing a steel tubular pile, 15 in. long embedded in a pressure chamber filled with saturated fine sand, as shown in Fig.(1.1). The pile is impact driven into the sand with known relative density under known confining pressure. The soil containing the pile is then subjected to a simulated seismic event. While the boundary confining pressure remain constant and drainage is permitted at the top boundary, pore water pressures, time-dependent pile head loads, and pile head movements were measured. Pore water pressure measurements were made at the mid-depth of the pile one diameter from the pile-soil interface and in the free field.

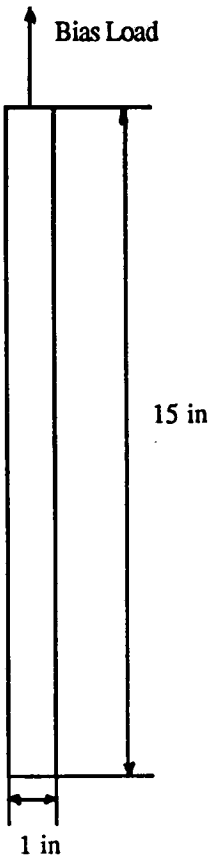

Fig.(1.1): Model Pile of Phase II, Oceanside Event Tests

CHAPTER (2)

METHOD OF ANALYSIS

CHAPTER (2)

METHOD OF ANALYSIS

The method of analysis applied in this work can be summarized in the following steps :

1- Construct the static p-y curves according to the current (1991) API criteria.

2- Degrade the static p-y curves by the degradation factor (ρ) proposed by Finn and Martin, (1979) and Kagawa and Kraft (1981c) ($\rho = (1 - r)^{1/2}$ where $r = \Delta u/\sigma'_v$). In this study, the static resistance p is multiplied by ρ to obtain the cyclic (seismic) resistance p, ($p = \rho p$).

3- Degrade the static t-z curves by the same degradation factor (ρ) applied to degrade the static p-y curves.

4- Analyze the pile under scaled axial cyclic loading using the computer program PAR (Pile Analysis Routines), PMB Systems (1988).

The above mentioned steps will be discussed in detail in the following :

1- The static p-y curves are constructed at each node along a prototype pile according the current API criteria (API, 1991). This can be done by generating these curves automatically using PAR and printing them out. It should be mentioned that choosing the generalized input in PAR necessiates entering all the load transfer curves (p-y, t-z, and q-z). The prototype pile is that which was scaled in the tests of Ochoa (1990).

2- The degradation factor (ρ) used in this analysis is that proposed by Finn and Martin, (1979), and Kagawa and Kraft (1981c).

With the absence of any measurements of pore water pressure changes around full-scale piles in sand during seismic events, the pore water pressure measured in Phase II, Oceanside event model tests are used to calculate the degradation factors. Those degradation factors are applied to both the static p-y and t-z curves.

3- The static t-z curves measured in Phase II, Oceanside event tests, are used as input to PAR, appropriately scaled from model to prototype are given in Appendix (A).

4- In this step the prototype pile is analyzed using the computer program PAR; the prototype pile is shown in Fig.(2.1). This step is subdivided into:

4.1- Input the load transfer curves. Instead of automatically generating load transfer curves at each node, they are input directly into the program (static p-y curves constructed according to current API criteria, and scaled measured t-z curves in Phase II, Oceanside event tests). Both the virgin and degraded curves are input to the program.

4.2- A static analysis if conducted first to determine the displacement under the bias load only, i.e., the displacement before the seismic event. The virgin p-y and t-z curves are used in this case.

4.3- Static and axial dynamic analyses are then performed to determine the displacement after the seismic event. The degraded p-y and t-z curves are used in this case.

4.4- The displacement computed after the simulated seismic event are then compared to those measured in the Phase II, Oceanside event tests. If the calculated and scaled measured displacements are equal, then the degradation factor for the t-z curve is correct, otherwise the degradation factor for the t-z curve only is varied until the measured and calculated displacements match. It should be noted that noted that no further degradation is made in the p-y curves, which are not significant in the axial dynamic analysis.

The nodal system and nodes at which unit load transfer curves were input are described in Appendix (A).

Before proceeding to the analysis using the computer program PAR, criteria for modeling the earthquake effect are presented.

Modeling the Earthquake Effect:

As PAR allows only for sinusoidal harmonic load at the pile head, and not loading from the soil as in the real earthquake loading, the measured force-time history at the pile head in Phase II, Oceanside event tests, are utilized to provide axial dynamic loading. The maximum measured force amplitude is then multiplied by a dynamic scaling factor (n_d^2 = 49) to obtain the maximum force amplitude in the prototype.

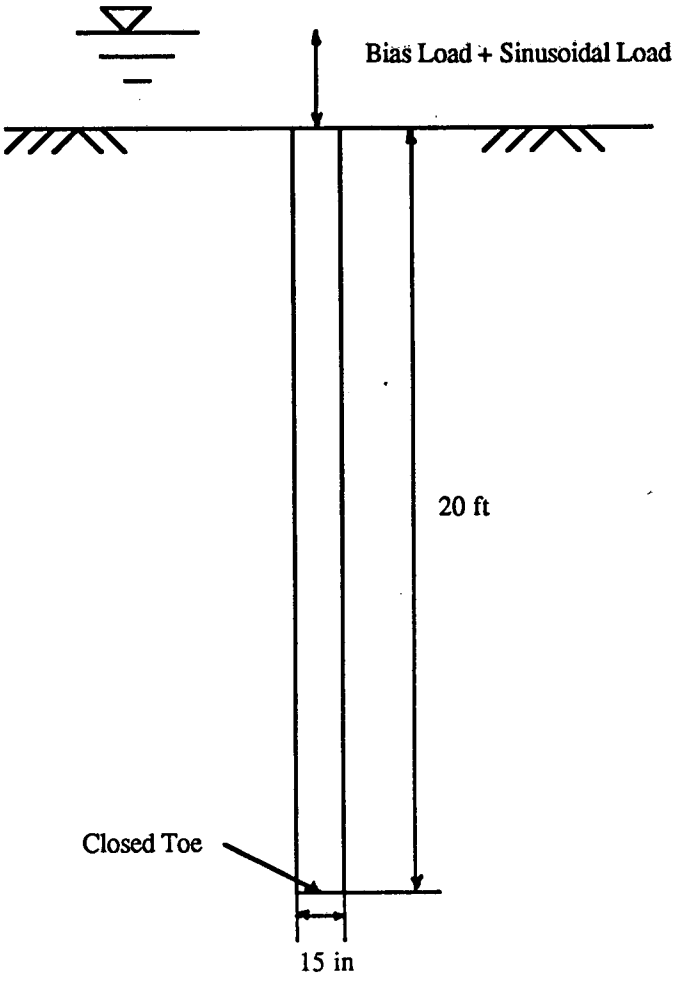

Fig.(2.1): Prototype Pile for PAR Analysis.

The irregular force-time history is then modeled by an equivalent number of uniform sinusoidal stress cycles. 10, 15, and 21 cycles are used for earthquake magnitudes of 7.0, 7.5, and 8.0 respectively, noting that those uniform stress cycles has an amplitude of 0.65 of the maximum amplitude (as per liquefaction analysis, Seed et al., 1975). Assuming that the duration of strong shaking will be 50 seconds in a magnitude 8.0 earthquake, the duration for earthquake magnitudes of 7.5 and 7.0 are then taken to be 35 and 25 seconds respectively. This is summarized in Table (2.1).

Table (2.1): Number of Uniform Stress Cycles and Duration for Different Earthquake Magnitudes, Seed et al. (1975).

Earthquake Magnitude (Richter)	No. of Uniform Stress Cycles at $0.65\,\tau_{max}$	Duration of Strong Shaking (Sec)
7.0	10	25
7.5	15	35
8.0	21	50

CHAPTER (3)
RESULTS

CHAPTER (3)
RESULTS

The results of this work are presented in the form of figures and tables with comments on some results.

Table (3.1) displays the values of r and of ρ determined in the model tests from measured pore water pressures at one pile diameter from the interface. ρ is observed to vary from 0.88 to 0.99. Tables (3.2) and (3.3) document the PAR input data from the prototype pile that was modeled computationally.

Table (3.1): Degradation Factors for Different Tests Calculated from Measured Pore Water Pressure Adjacent to the Model Pile in Phase II, Oceanside event tests.

Test	PWP u (psi)	PWP Ratio $r = u/\sigma_c$	D. F. $\rho = (1 - r)^{1/2}$
R1	0.220	0.088	0.960
R2	0.120	0.048	0.970
S1	0.107	0.043	0.980
S3	0.174	0.069	0.960
S4	0.060	0.024	0.990
U1	0.188	0.200	0.890
U2	0.125	0.141	0.930
U3	0.500	0.223	0.880

PWP = Pore water pressure

D.F. = Degradation factor

σ_c = Effective isotropic confining pressure.

Table (3.2) Input Data for the Static Analysis (D_r = 55%, and σ_c = 2.5 psi).

Test	Static Capac. Model (lb)	Static Capac. Prototype[1] (Kips)	Bias Load Model (lb)	Bias Load Prototype (Kips)	Percentage of Inferred Static Capac.
R1	96.00	21.66	73.00	16.425	76.00
R2	108.00	24.30	93.00	20.430	86.00
S1	135.00	30.38	85.00	19.125	63.00
S3	108.00	24.30	83.00	18.675	77.00
S4	104.00	23.40	95.00	21.375	91.00
U1	77.00	17.33	35.00	7.880	45.00
U2	112.00	25.20	72.00	16.200	64.00
U3	96.00	21.60	112.00	16.875	78.00

D_r = Relative density

σ_c = Effective isotropic confining pressure

Static scaling factor n_s = 15

1 See Appendix (B).

Table (3.3): Input Data for the Dynamic Analysis of the Prototype Pile.

Test	Earthquake Magnitude	Duration (sec)	Amplitude of Sine Force (Kips)	No. of Significant Cycles	Period (sec)	Frequency (Hz)
R1	7.0	25.00	0.225	10	2.500	0.4000
R2	7.0	25.00	0.280	10	2.500	0.4000
S1	7.5	35.00	0.176	15	2.333	0.4286
S3	7.5	35.00	0.425	15	2.333	0.4286
S4	7.5	35.00	0.153	15	2.333	0.4286
U1	8.0	50.00	0.686	21	2.381	0.4200
U2	8.0	50.00	0.408	21	2.381	0.4200
U3	8.0	50.00	0.539	21	2.381	0.4200

Dynamic scaling factor n_d^2 = 49.

Table (3.4) shows the measured and calculated degradation factors for Phase II, Oceanside event tests. In all the tests, ρ in the t-z curves was less than that in the p-y curves, indicating a more severe degradation in the t-z curves as expected.

Table (3.4): Degradation Factors Before and After the Dynamic Analysis of the Prototype Pile.

Test	δ^1 Calculated in static analysis (ft)	δ^2 Calculated after dyna. Analysis[2] (ft)	(ρ) Equal in p-y & t-z	δ^3 Calculated ρ equal in p-y & t-z (ft)	(ρ) matched in t-z only	δ Measured (model) (in)	δ Calculated (model) (in)
R1	0.00347	0.00421	0.960	0.00698	0.820	0.0060	0.0060
R2	0.00432	0.00627	0.970	0.01430	0.880	0.0450	0.0171
S1	0.00261	0.00298	0.980	0.00358	0.920	0.0017	0.0017
S3	0.00323	0.00387	0.960	0.00779	0.790	0.0100	0.0080
S4	0.00363	0.00776	0.990	0.00425	0.940	Failure	Failure
U1	0.00126	0.00214	0.890	0.00239	0.850	0.0020	0.0020
U2	0.00375	0.00555	0.930	0.00974	0.740	0.0100	0.0100
U3	0.00442	0.00711	0.880	0.01620	0.790	Failure	Failure

δ is the axial pile head displacement.

1 Static displacement under bias load only.

2 Displacement after dynamic analysis with degradation factors in t-z curves set equal to those in p-y curves.

3 Displacement after dynamic analysis with degradation factors in t-z curves reduced to match the model displacement.

Some comments are made on tests R2, S3, S4, and U3. In test R2, reducing the degradation factor by 1% more (i.e. D.F. = 0.87) resulted in failure of the pile and the calculations stopped in the static analysis. As can be seen from Table (3.4), the measured and calculated displacements do not match. So, the degradation factor in the t-z curves for this test should be less than 0.88. The same behavior occurred in test S3, but the actual degradation factor will not be considerably less than 0.79.

21

The actual degradation factors in tests S4 and U3, in which failure occurred, are not known because failure occurred during the earthquake shaking, which prevented using displacement matching as a measure of calculating ρ.

In test S4, the static and dynamic analyses were completed at a degradation factor of 0.95, and gave displacements in the mobility zone (0.012 in), the mobility zone is defined by Ochoa as model displacements in the range of 0.007 in to 0.45 in (Ochoa, 1990). Reducing this factor to 0.94 resulted in failure of the pile, and the calculations stopped in the dynamic analysis. The same behavior occurred in test U3, with calculations stopped in the dynamic analysis. It should be noted that the calculated displacements in the prototype were converted into those in the model by dividing them by the dynamic scaling factor ($n_d = 7$) and multiplying them by 12 to covert from feet to inch.

A sample printout of the deformed shape of the pile is provided in Fig.(3.1) for displacements after the static analysis, after the dynamic analysis with degradation factors equal in both p-y and t-z curves, and after the dynamic analysis with degradation factors reduced only in the t-z curves to match the model displacements.

Figure (3.2) shows the relation between the earthquake magnitude and the degradation factors for Phase II, Oceanside event tests. It could be noticed from the figure that there is not much difference between the degradation factors for earthquake magnitudes of 7.0 and 7.5. However, there is a pronounced decrease in the degradation factors for earthquake magnitude of 8.0.

Figure (3.3) shows the relation between amount of bias load relative to the pile capacity, expressed in percentage, and the degradation factors. This figure gives a more clear picture for degradation in t-z curves because it accounts for the applied bias load for different earthquake magnitudes. Again, it can be seen that the difference between the effects of earthquake magnitudes 7.0 and 7.5 is not significant, while for earthquake magnitude of 8.0, the degradation is more severe. It should be noted that the points at which failure occurred were not considered in drawing the linear relation because the model and prototype displacements could not be matched.Figure (3.3) appears to be a reasonable preliminary criterion for analysis of prototype piles for axial loading for a seismic event similar to the Oceanside (1986).

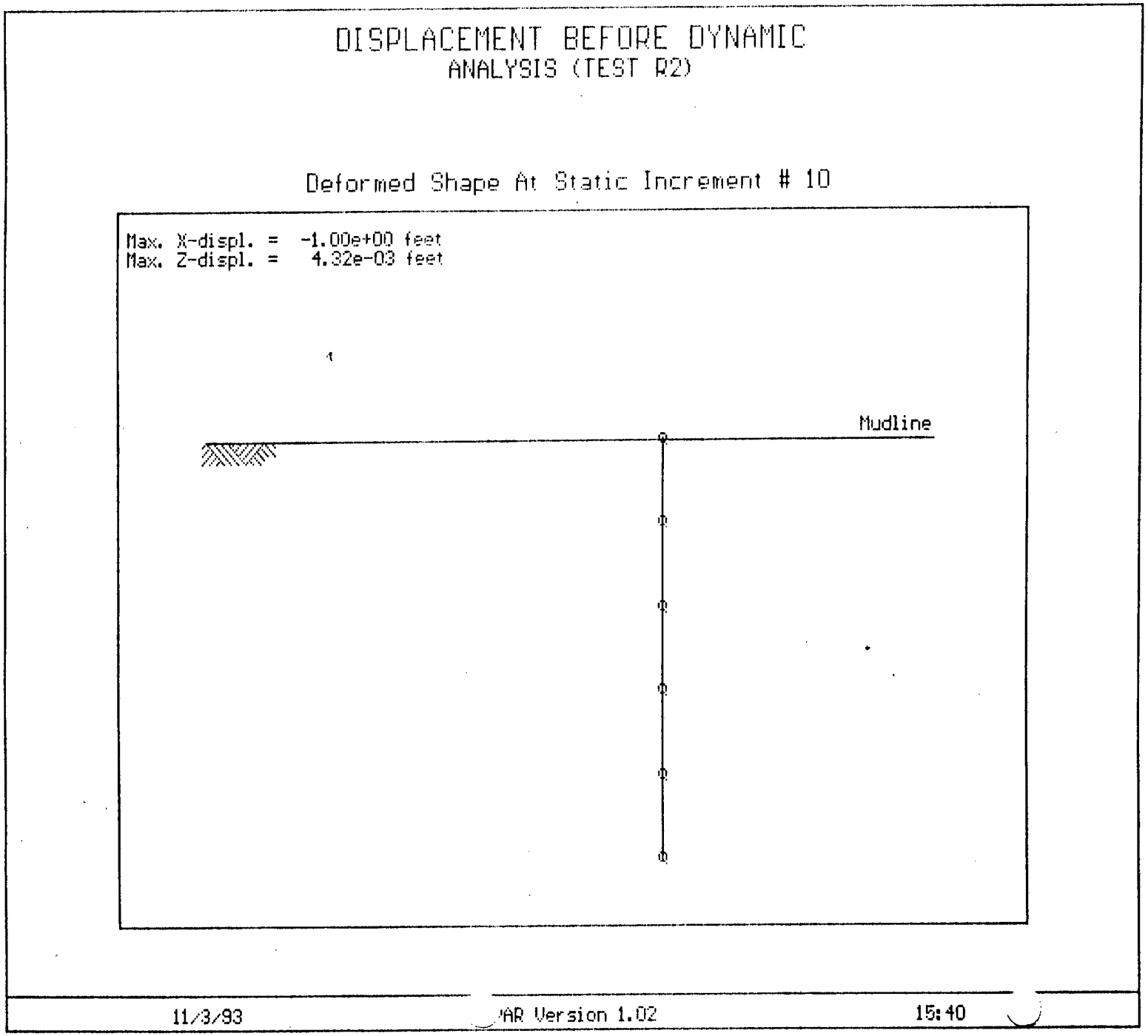

Fig.(3.1a): Deformed Shape of the Pile After the Static Analysis.

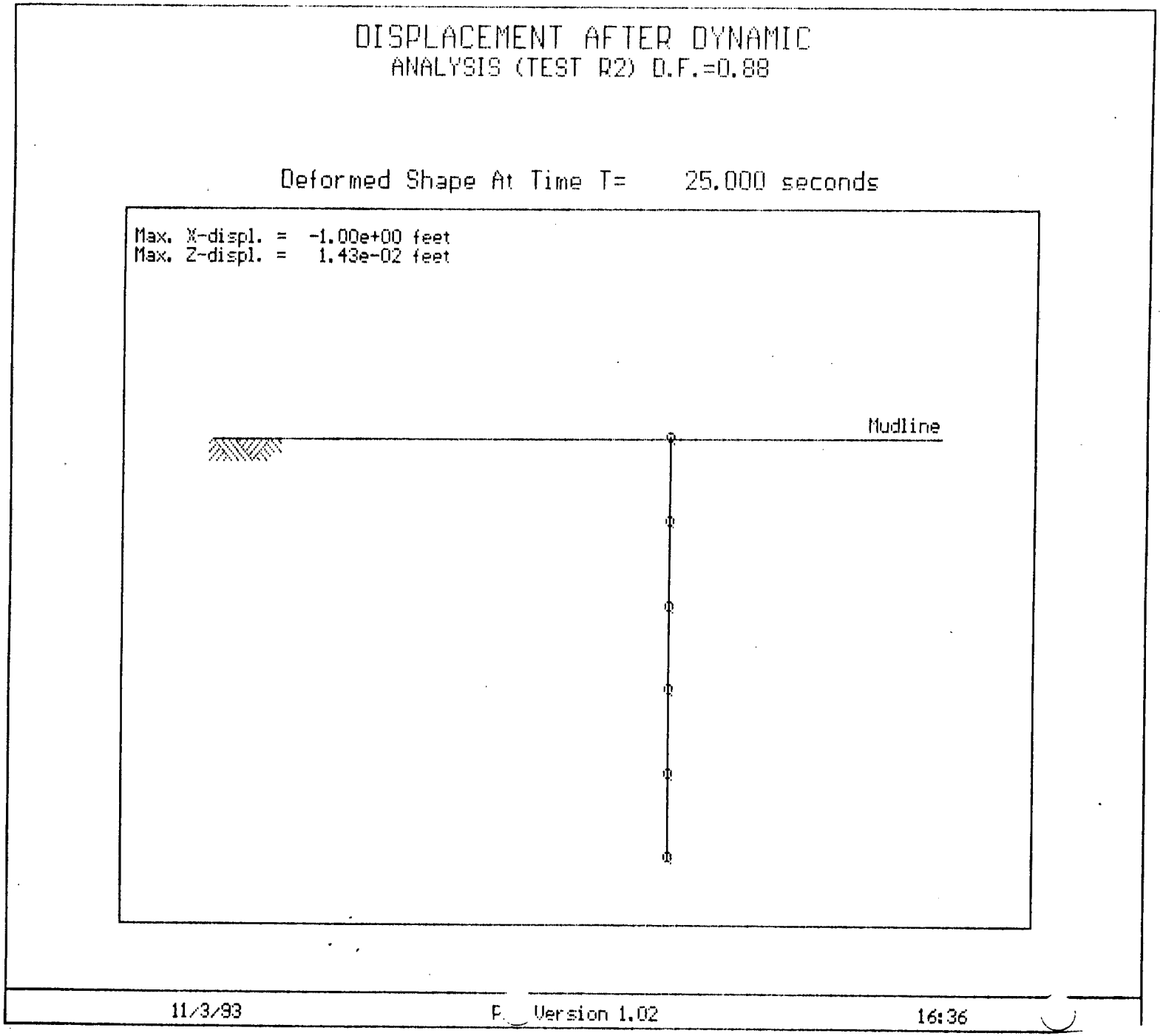

Fig.(3.1b): Deformed Shape of the Pile After the Dynamic Analysis with p Equal in Both p-y and t-z Curves.

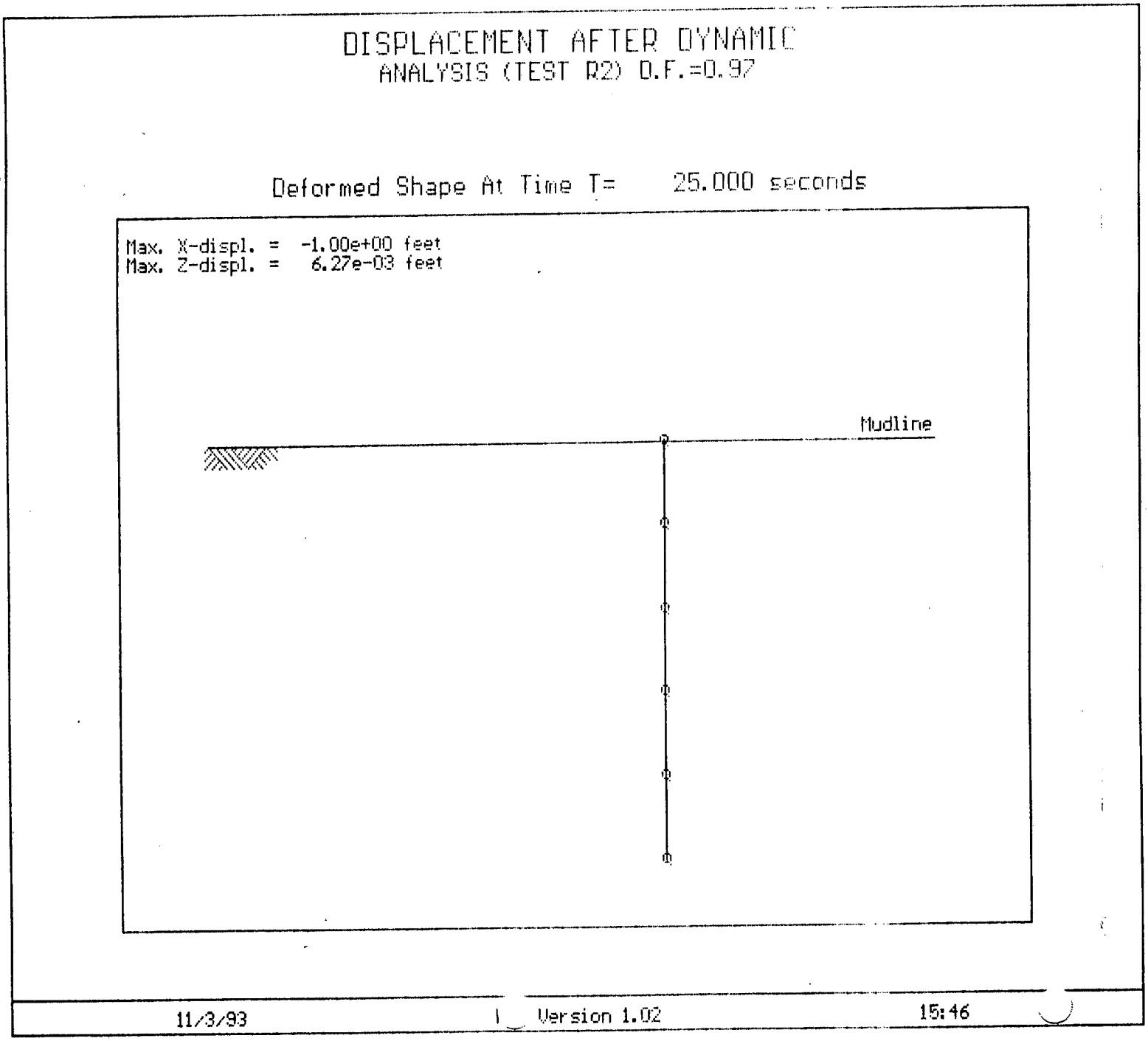

Fig.(3.1c): Final Deformed Shape of the Pile with Displacements Matched in Both Model and Prototype.

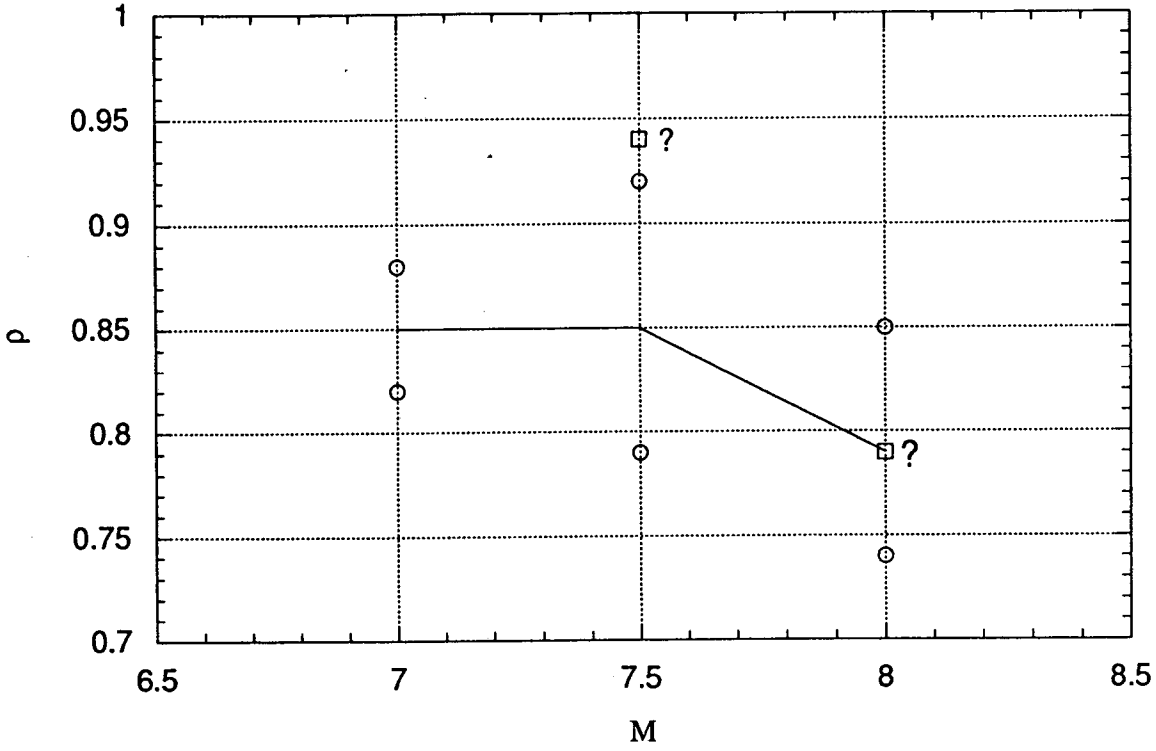

Fig.(3.1): Relation between Earthquake Magnitude (M) and Degradation Factors (ρ).

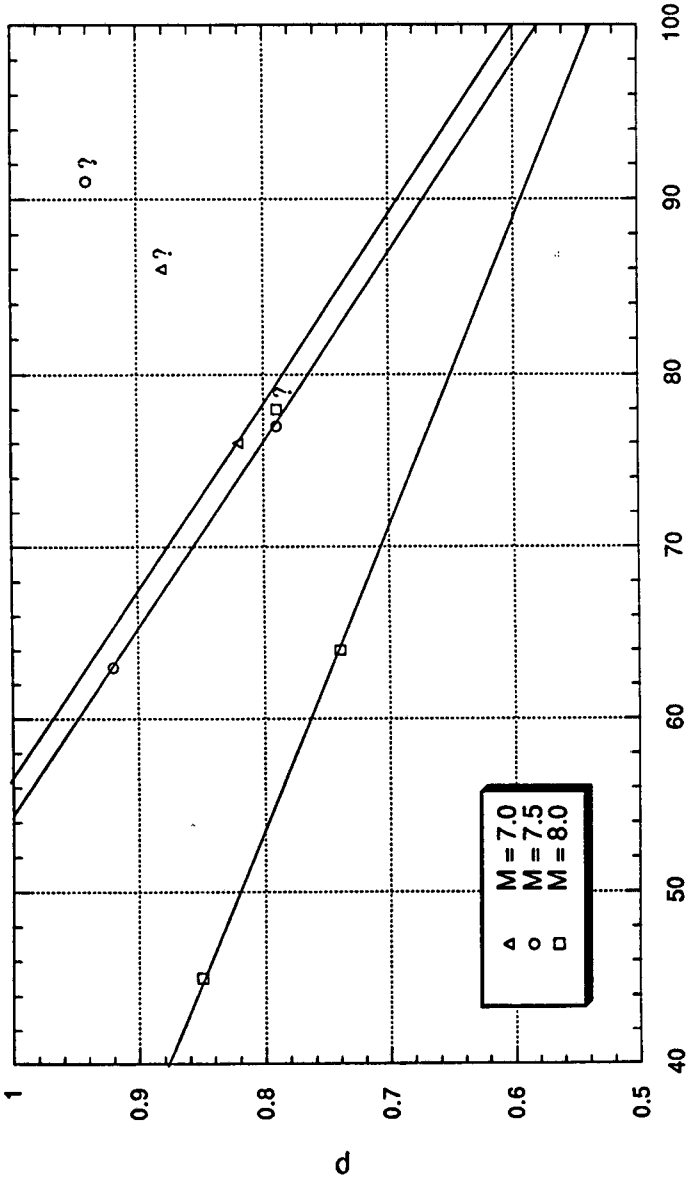

Fig.(3.3): Relation between Bias Load, Expressed as Percentage of Static Capacity, and the Degradation Factors (ρ) for Different Earthquake Magnitudes.

REFERENCES

REFERENCES

1- API, (1991), "Recommended Practice for Planning, Designing and Constructing Fixed Offshore Platforms", American Petroleum Institute, API RP2A, 19th Edition.

2- Cox, W.R.; Reese, L.C.; and Grubbs, B.R., (1974), "Field Testing of Laterally Loaded Piles in Sand", Proceedings of the 6th Offshore Technology Conference, Houston, Vol.2, Paper No.2079, pp.459-472.

3- Finn, W.D.L., and Martin, G.R., (1979), "Analysis of Piles Foundations for Offshore Structures Under Wave and Earthquake Loading", Proceedings of the 2nd International Conference on Behavior of Off-Shore Structures, Imperial College, London, England, Paper No.38, pp.497-502.

4- Kagawa, T., (1980), "Soil-Pile-Structure Interaction of Offshore Structures During an Earthquake", Proceedings of the 12th Annual Offshore Technology Conference, Houston, Vol.2, Paper No.3820, pp.235-245.

5- Kagawa, T., and Kraft, L.M., (1980a), "Lateral Load-Deflection Relationships of Piles Subjected to Dynamic Loadings", Soils and Foundations, Vol.20, No.4, pp.19-36.

6- Kagawa, T., and Kraft, L.M., (1980b), "Seismic P-Y Responses of Flexible Piles", ASCE, Journal of the Geotechnical Engineering Division, Vol.106, No.GT8, pp.899-918.

7- Kagawa, T., and Kraft, L.M., (1981a), "Dynamic Characteristics of Lateral Load-Deflection Relationships of Flexible Piles", International Journal of Earthquake Engineering and Structural Dynamics, Vol.9, No.1, pp.53-68.

7- Kagawa, T., and Kraft, L.M., (1981b), "Modeling the Liquefaction Process", ASCE, Journal of the Geotechnical Engineering Division, Vol.107, No.GT12, pp.1593-1607.

8- Kagawa, T., and Kraft, L.M., (1981c), "Lateral Pile Response During Earthquakes", ASCE, Journal of the Geotechnical Engineering Division, Vol.107, No.GT12, pp.1713-1731.

10- Matasovic, N., and Vucetic, M., (1992), "Modeling of the Cyclic Stress-Strain Behavior of Liquefiable Sands", Research Report, Department of Civil Engineering, University of California, Los Angeles.

11- Matlock, H., and Foo, S.H.C., (1979), "Axial Analysis of Piles Using Hysteretic and Degrading Soil Model", Proceedings of the 1st International Conference on Numerical Methods in Offshore Piling, Institution of Civil Engineers, London, pp.127-133.

12- Matlock, H.; Foo, S.H.C.; and Bryant, L.M., (1978), "Simulation of Lateral Pile Behavior Under Earthquake Motion", Earthquake Engineering and Soil Dynamics, Proceedings of the ASCE Specialty Conference, Pasadena, California, Vol.2, pp.600-619.

13- Ochoa, M., (1990), "Response of Tension Piles to Simulated Seismic Motion in Saturated Fine sand", PhD Dissertation Presented to the Civil and Environmental Engineering Department, University of Houston, Houston, Texas.

14- PAR, (1988), "Pile Analysis Routines", PMB Engineering Software, San Francisco, California.

15- Poulos, H.G., (1988), "Marine Geotechnics", Unwin Hyman Ltd., London.

16- Reese, L.C.; Cox, W.R.; and Koop, F.D., (1974), "Analysis of Laterally Loaded Piles in Sand", Proceedings of the 6th Offshore Technology Conference, Houston, Vol.2, Paper No.2080, pp.473-483.

17- Seed, H.B.; Idriss, I.M.; Makdisi, F.; and Banerjee, N., (1975), "Representation of Irregular Stress Time Histories by Equivalent Uniform Stress Series in Liquefaction Analysis", Earthquake Engineering Research Center, Report No. EERC 75-29, University of California, Berkeley.

18- Seed, H.B.; Wong, R.T.; Idriss, I.M.; and Tokimatsu, K., (1986), "Moduli and Damping Factors for Dynamic Analysis of Cohesionless Soils", ASCE, Journal of the Geotechnical Engineering Division, Vol.112, No.11, pp.1016-1032.

APPENDIX (A)

SCALING THE T-Z CURVES

APPENDIX (A)
SCALING THE T-Z CURVES

As it is intended to reproduce the results of Phase II, Oceanside event tests, the t-z curves are constructed using the following procedure:

The t-z curves along the pile length are not provided from the model tests, only the load-displacement relationships at the pile head are provided. So, the measured load-displacement values in the model are converted first to those of the prototype by multiplying the load by square of the static scaling factor (n_s^2) and the displacement by the static scaling factor (n_s).

In the prototype, it is assumed that the distribution of skin friction along the pile length is triangular and the area of the triangle is the load on the pile head. This triangle is then subdivided into the desired number of elements (5 elements in this case), as shown in Fig.(A-1). The area of each element in the triangle will represent the amount of skin friction that will be lumped into the node. Those areas are : 0.01, 0.08, 0.16, 0.24, 0.32, and 0.19, respectively (with a total of 1.00) i.e., the first node will provide 1% of the total load, the second one will provide 8% of the total load, and so on. For a rigid pile, the displacements at all the nodes will be the same, so, at any known displacement the axial soil reaction at the pile head load at the pile head is multiplied by the above areas to give the load at each node. Thus, establishing the t-z curves at all the pile nodes.

For example, in test R1 (prototype), the t-z curve at node 1 is constructed as follows:

The displacement w_{p1} is the same as w_p (at the pile head) (i.e., 0.000238, 0.000513, 0.000875 ft and so on) and the load transferred at node 1, f_{p1}, is 1% of the total load on the pile (1% of f_{pt}, i.e., 0.022275, 0.054225, 0.092925 Kips and so on). At node 2, the displacements are also the same but the total load f_{pt} is multiplied by 8% and so on, as shown in Table (A-1).

Measured static t-z curves in Phase II, Oceanside event model and the corresponding prototype values for different tests are given in the following tables.

32

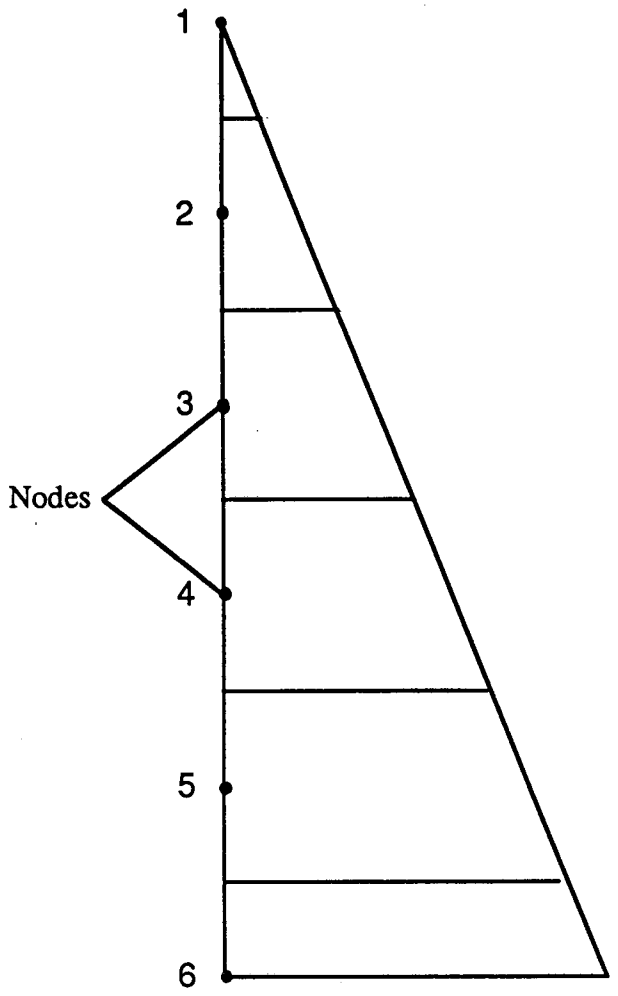

Fig.(A-1): Distribution of Load in Different Elements of the Pile,
The Pile is Divided into 5 Elements and 6 Nodes.

Test (R1)

Model Dis. w_m (in)	Model Load f_m (lb)	Prot. Dis. w_p (ft)	Prot. Load f_p (Kips)
0.00019	9.90	0.000238	2.2275
0.0041	24.10	0.000513	5.4225
0.0007	41.30	0.000875	9.2925
0.00109	49.0	0.001363	11.025
0.00182	60.0	0.002275	13.5
0.00218	68.0	0.002725	15.30
0.00267	73.0	0.003338	16.425
0.004	83.40	0.005	18.765
0.0065	96.0	0.008125	21.60

Table (A-1): T-z Curves of the Prototype at the Pile Nodes for Test R1.

Prot. Disp. w_p (ft)	Total load on prot. f_{pt} (Kips)	f_p at node No. 1 0.01 f_{pt} (Kips)	f_p at node No. 2 0.08 f_{pt} (Kips)	f_p at node No. 3 0.16 f_{pt} (Kips)	f_p at node No. 4 0.24 f_{pt} (Kips)	f_p at node No. 5 0.32 f_{pt} (Kips)	f_p at node No. 6 0.19 f_{pt} (Kips)
0.000238	2.2275	0.022275	0.17820	0.35640	0.53460	0.71280	0.42323
0.000513	5.4225	0.054225	0.43380	0.86760	0.1.3014	1.73520	1.03028
0.000875	9.2925	0.092925	0.74340	1.46860	2.23020	2.97360	1.76558
0.001363	11.0250	0.110250	0.88200	1.76400	2.64600	3.52800	2.09475
0.002275	13.500	0.135000	1.08000	2.16000	3.24000	4.32000	2.56500
0.002725	15.300	0.153000	1.22400	2.44800	3.67200	4.89600	2.90700
0.003338	16.425	0.164250	1.31400	2.62800	3.94200	5.25600	3.12075
0.005000	18.765	0.187650	1.50120	3.00240	4.50360	6.00480	3.56535
0.000813	21.600	0.216000	1.72800	3.45600	5.18400	6.91200	4.10400

Test (R2)

Model Dis. w_m (in)	Model Load f_m (lb)	Prot. Dis. w_p (ft)	Prot. Load f_p (Kips)
0.00036	16.0	0.00045	3.60
0.00073	45.0	0.000913	10.125
0.00145	64.0	0.001813	14.40
0.00164	73.0	0.00205	16.425
0.00255	84.0	0.003188	18.90
0.00327	93.0	0.004088	20.925
0.008	104.0	0.0100	23.40
0.0116	108.0	0.0145	24.30

Test (S1)

Model Dis. w_m (in)	Model Load f_m (lb)	Prot. Dis. w_p (ft)	Prot. Load f_p (Kips)
0.00018	12.0	0.000225	2.70
0.00105	43.0	0.001313	9.675
0.00122	57.0	0.001525	12.825
0.00142	65.0	0.001775	14.625
0.00158	73.0	0.001975	16.425
0.00178	79.0	0.002225	17.775
0.0020	85.0	0.0025	19.125
0.00418	110.0	0.005225	24.75
0.00864	135.0	0.0108	30.375

Test (S3)

Model Dis. w_m (in)	Model Load f_m (lb)	Prot. Dis. w_p (ft)	Prot. Load f_p (Kips)
0.00024	13.8	0.0003	3.105
0.00053	20.8	0.000663	74.680
0.00109	41.3	0.001363	9.2925
0.00145	54.2	0.001813	12.195
0.0017	68.0	0.002125	15.30
0.00206	76.1	0.002575	17.1225
0.0024	83.2	0.003	18.720
0.0038	96.2	0.00475	21.645
0.0061	108.0	0.007625	24.300

Test (S4)

Model Dis. w_m (in)	Model Load f_m (lb)	Prot. Dis. w_p (ft)	Prot. Load f_p (Kips)
0.00015	10.0	0.000188	2.250
0.00029	19.0	0.000363	2.275
0.00058	32.0	0.000725	7.200
0.00073	44.0	0.000913	9.900
0.0013	53.5	0.001625	12.048
0.00145	63.0	0.001813	14.175
0.00218	79.0	0.002725	17.775
0.00254	90.5	0.003175	20.363
0.00982	104.0	0.012275	23.400

Test (U1)

Model Dis. w_m (in)	Model Load f_m (lb)	Prot. Dis. w_p (ft)	Prot. Load f_p (Kips)
0.00018	10.0	0.000225	2.250
0.00048	17.7	0.0006	3.983
0.00073	28.0	0.000913	6.300
0.00097	35.3	0.001213	7.943
0.00157	40.5	0.001963	9.113
0.00303	55.2	0.003788	12.42
0.00461	67.2	0.005763	15.120
0.00606	71.1	0.007575	16.00
0.0080	77.0	0.010	17.325

Test (U2)

Model Dis. w_m (in)	Model Load f_m (lb)	Prot. Dis. w_p (ft)	Prot. Load f_p (Kips)
0.00024	13.8	0.0003	3.105
0.0053	29.3	0.000663	6.5925
0.00097	42.7	0.001213	9.6075
0.00157	54.3	0.001963	12.218
0.0022	62.9	0.00275	14.16
0.0026	68.1	0.00325	15.323
0.0032	72.2	0.004	16.245
0.0068	95.7	0.0085	21.533
0.0104	112.0	0.013	25.200

Test (U3)

Model Dis. w_m (in)	Model Load f_m (lb)	Prot. Dis. w_p (ft)	Prot. Load f_p (Kips)
0.00018	10.0	0.000225	2.25
0.00052	22.0	0.00065	4.95
0.00073	31.0	0.000913	6.98
0.0013	42.0	0.00163	9.45
0.0018	51.0	0.00225	11.48
0.0025	61.0	0.00313	13.73
0.0034	75.0	0.00425	16.88
0.0072	96.0	0.009	21.60

APPENDIX (B)

STATIC p-y Curves

APPENDIX (B)

STATIC p-y CURVES

The static and cyclic p-y curves are presented in this part. Fig.(B-1) shows the static p-y curves constructed using the criteria of Reese et al. (1974), Kagawa and Kraft (1981c), and the Recent API criteria (API, 1991). These curves are drawn for the case study given by Reese et al., 1974 (Mustang Island Tests) which Kagawa and Kraft (1981c) used to compare their static curve with it. As can be seen from the figure their curve was well lower than the old and recent API criteria.

Figure (B-2) shows the static p-y curves for the prototype pile of our study drawn using the current API criteria and that of Kagawa and Kraft (1981c). Again their curve was well below that of the API.

It could be concluded from the figures that the p-y curve of Reese et al., 1974 was not correctly represented in Kagawa and Kraft Paper in 1981.

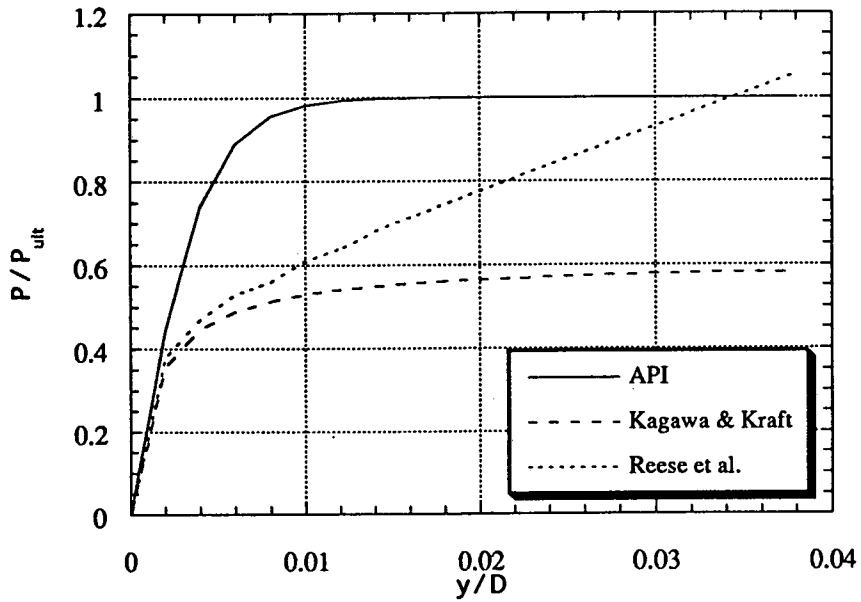

Fig.(B-1): Static Recent API, Kagawa & Kraft, and Reese et al. P-Y Curves for the Mustang Island Study. (D=2ft, ϕ=39°, z=6ft, K_o=0.4).

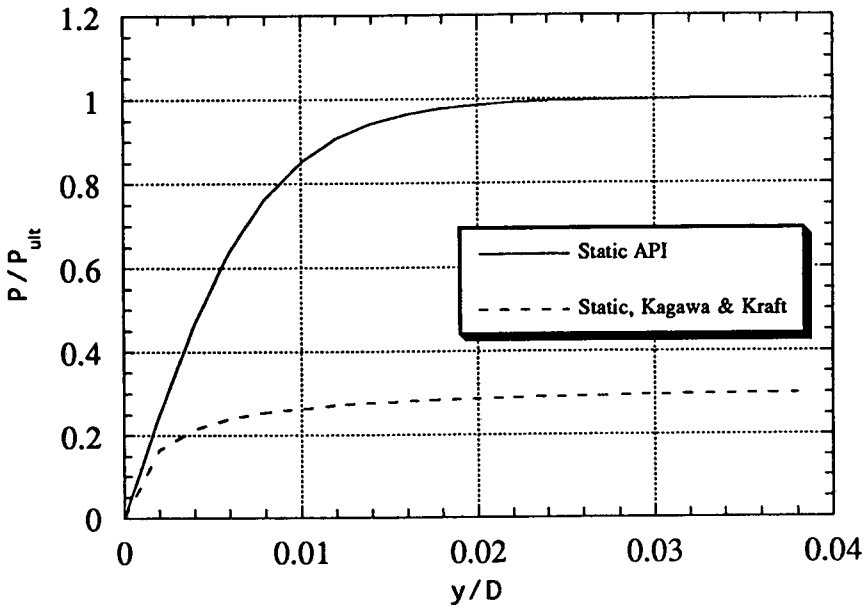

Fig.(B-2): Static p-y Curves for Recent API and Kagawa and Kraft (1981c) for the Prototype Pile.

Appendix II

M.M.S. PROJECT

I. Prelimnary Tests

Objectives :

The objectives of these tests were to establish a proper testing protocol and to verify its effectiveness by confirming existing results obtained with the July 13th 1986 Oceanside earthquake.

Test Details :

1. Static and dynamic tests were conducted in microfine sand under 2.5 psi confining pressure and at moderate relative densities of about 55 %. These have been tabulated in Tables 1 & 2. Certain static tests were conducted solely with the intention of developing a calibration curve of blow count vs. static capacity. These are referred to by letter 'S' in parenthesis following the test number.

2. Due to scatter obtained in the calibration curve, an alternate approach was used to establish the baseline static capacity for the given test condition. The pile was driven by impact into place, then a static uplift load test was conducted on the pile. The point of initial slip was interpreted to be as the failure point. Subsequent to failure of the pile, the pile was restruck with a single blow using a smaller compaction hammer. This was followed by another uplift load test under existing conditions.

3. All the three dynamic tests in this phase were conducted with the **July 13th 1986 Oceanside Earthquake Event**

Results :

1. In spite of scatter in the ultimate load capacities of the piles under identical testing conditions, it was observed that movement corresponding to slip or failure for most cases ranged from 0.005 - 0.007 in. which confirmed that the zones for stability, mobility and failure are governed by the movement of the pile. (See Fig. 1.0)

2. The capacity of a restruck pile , driven with an additional blow subsequent to failure (defined at initial slip) after initial baseline uplift test was within +/- 10% of the initial baseline static capacity. (See Fig. 2.0 and Table 1.0)

3. Load transfer was higher in the bottom half of the pile than in the upper half. A typical computed f-z curve has been attached (See Fig. 3.0).

4 Stability, Mobility and Failure zones established by Ochoa for the July 13th Oceanside Earthquake record were verified for the given conditions (See Fig. 4.0). Static and Dynamic Data obtained during the testing sequence have also been attached. (See Fig. 5.0 to Fig. 17.0)

Table 1.0 - Static Load Tests

Test No	Blow Count (blows/in.)	Initial Static Capacity (lb)	Uplift Capacity after addl. blow (lb)
T#9(S)	3	180.1	-
T#10(S)	3.6	182.1	-
T#7(SD)	6.3	136.8	-
T#8(SD),T#8(SDR)	4	177.3	158.2
T#9(SD),T#9(SDR)	3	95.9	105.6
T#10(SD),T#10(SDR)	6	198.6	182.5
T#12(SD),T#12(SDR)	5.6	173.8	189.7

** All tests were conducted in micro-fine sand, deposited at about 55% rel. density and 2.5 psi confining pressure.

Table 2.0 - Dynamic Tests

*Test No	Blow count.	Eq. Mag. (a)	Predicted Static Capacity (b)	(c)	Bias Load (d)	Post Shaking Capacity (lbs)	Movement (in.)	Loss or gain in Capacity (%)	Condition
T#9(SD)	3	7.0	95.0	116.2	65	115.4	0.0019	0.65 (loss)	Stability
T#14(SD)	3.3	8.0	148.9	182.0	62	183.0	0.1	0.52 (gain)	Mobility
T#13(SD)	2.7	8.0	101.2	123.6	92	0	pull out	100 (loss)	Failure

* All tests were conducted in micro-fine sand, deposited at about 55% rel. density and 2.5 psi confining pressure
(a) - Richter Magnitude of the Applied Earthquake
(b) - Predicted Static Capacity in lb computed as 10% lower than the baseline static capacity
(c) - Predicted Static Capacity in lb computed as 10% higher than the baseline static capacity
(d) - Applied bias loading as % of (c)

Notations used inside the parenthesis

S - refers to static tests only i.e. a single static load test was conducted on the pile. The pile was not restruck or subjected to dynamic event during that test

SD - refers to static cum dynamic tests i.e. in this test the pile was subjected to dynamic event with a certain tension bias load on the pile. Also, if 'R' is included along with notation it implies that after the baseline static test, the pile was restruck with an addl. blow and a uplift load test conducted to confirm the validity of the new approach followed.

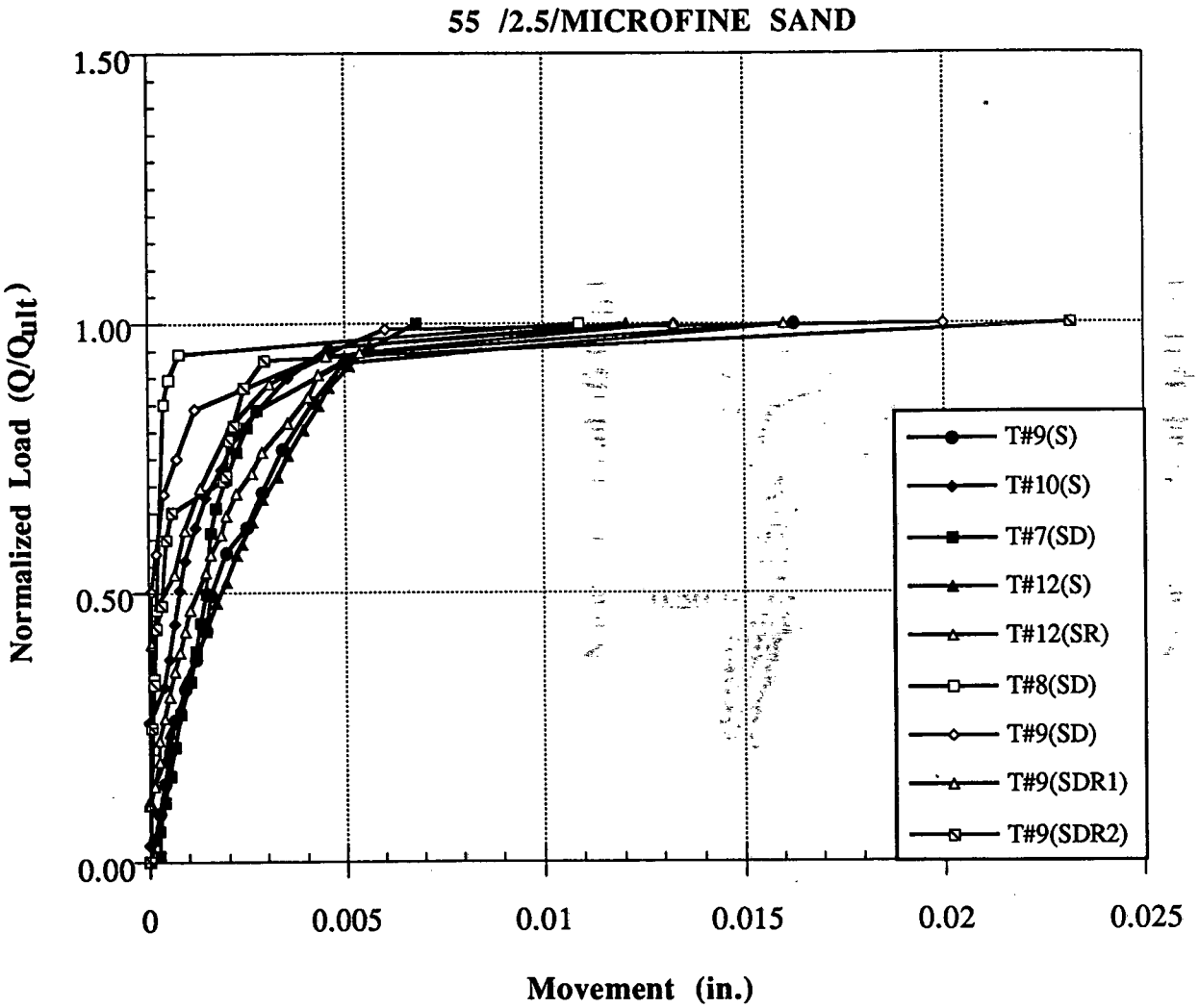

Fig. 1.0 : Static Load Test Curves, Normalized By Ultimate Load

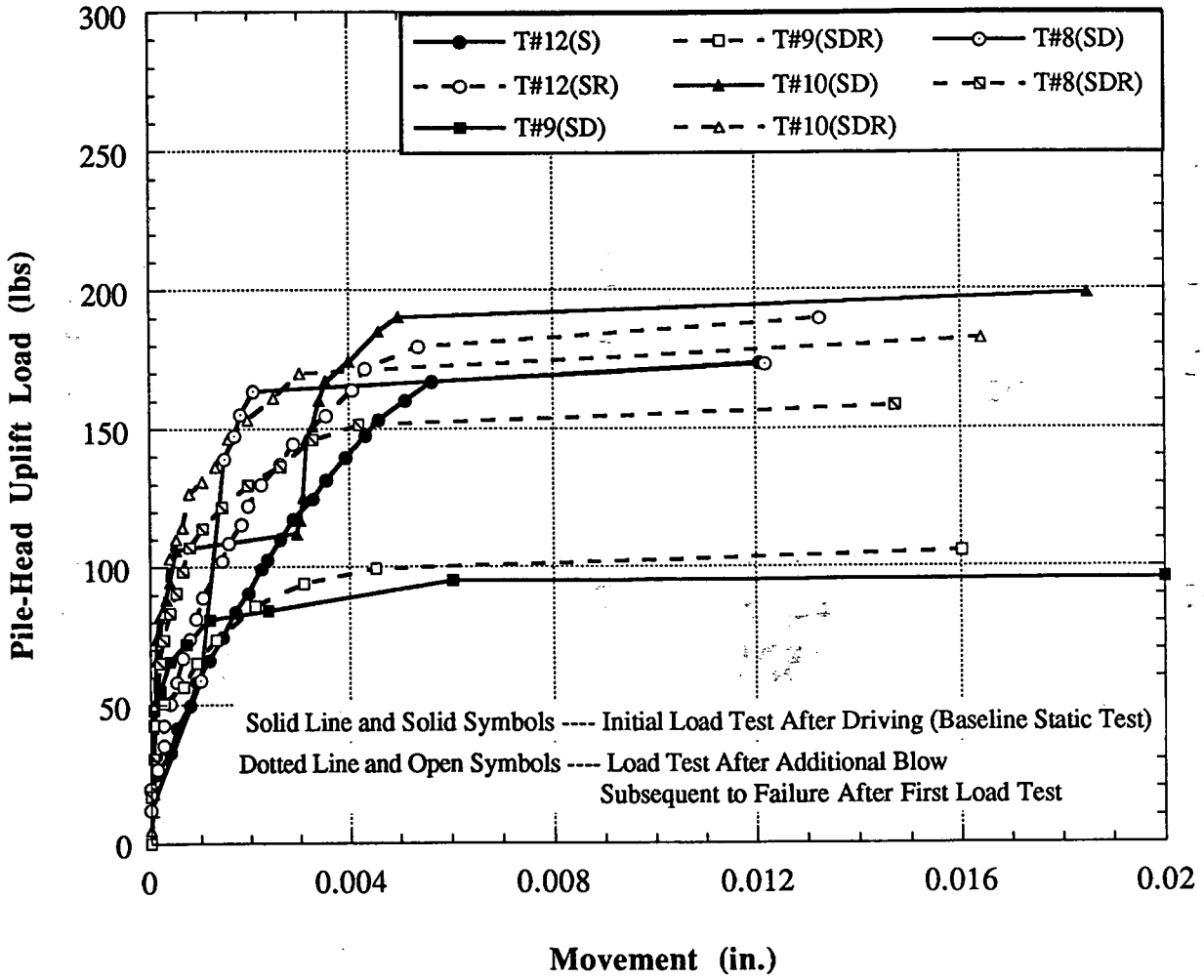

Fig. 2.0 : Variation in the Static Capacity due to Restriking the Pile with an Additional Hammer Blow

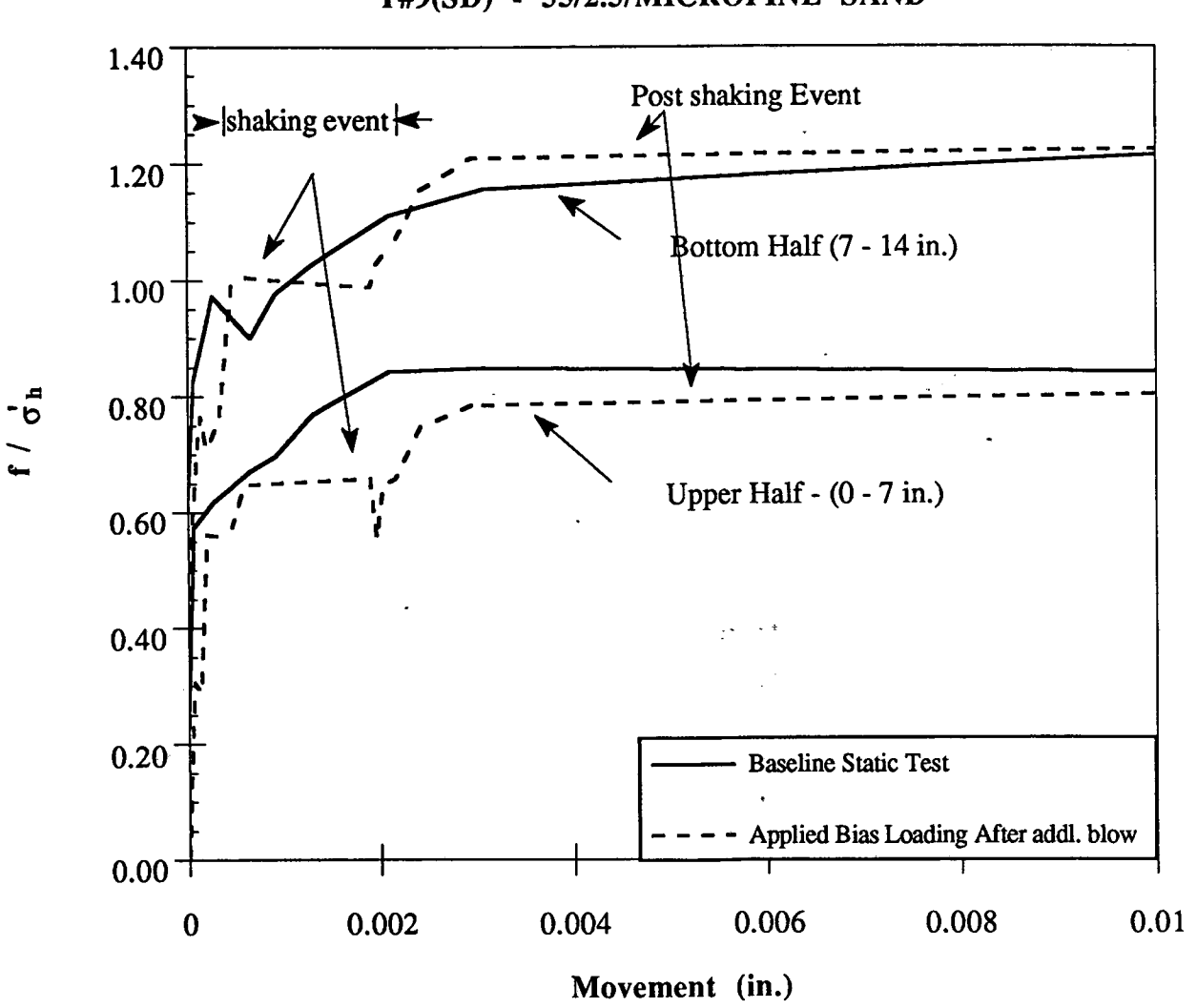

Fig. 3.0 : Typical Unit Shaft Friction Vs. Movement Relationship

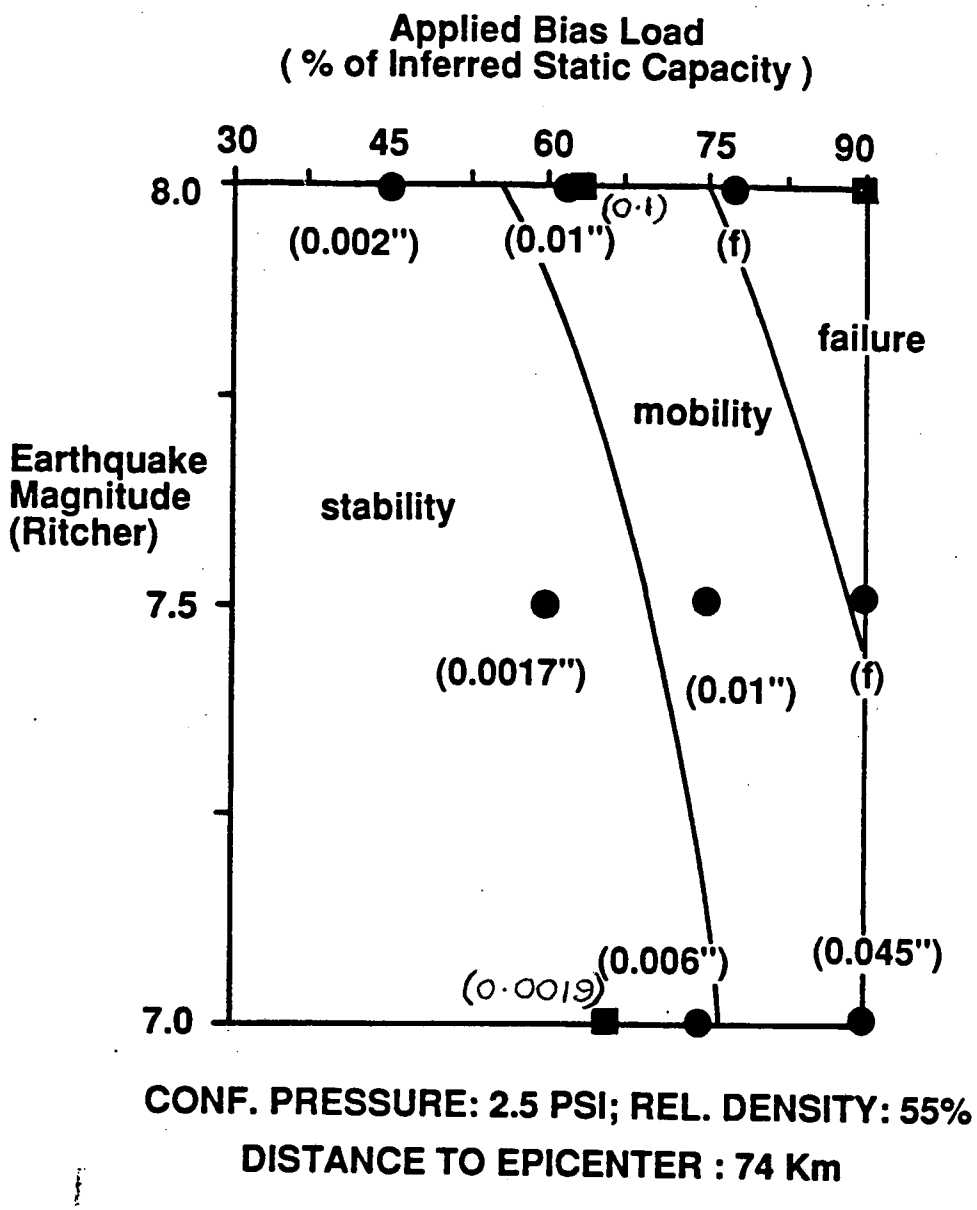

Fig. 4.0 : Stability , Mobility and Failure Zones for 55% Rel. Density, 2.5 psi Confining Pressure with the July 13th 1986 Oceanside Event.

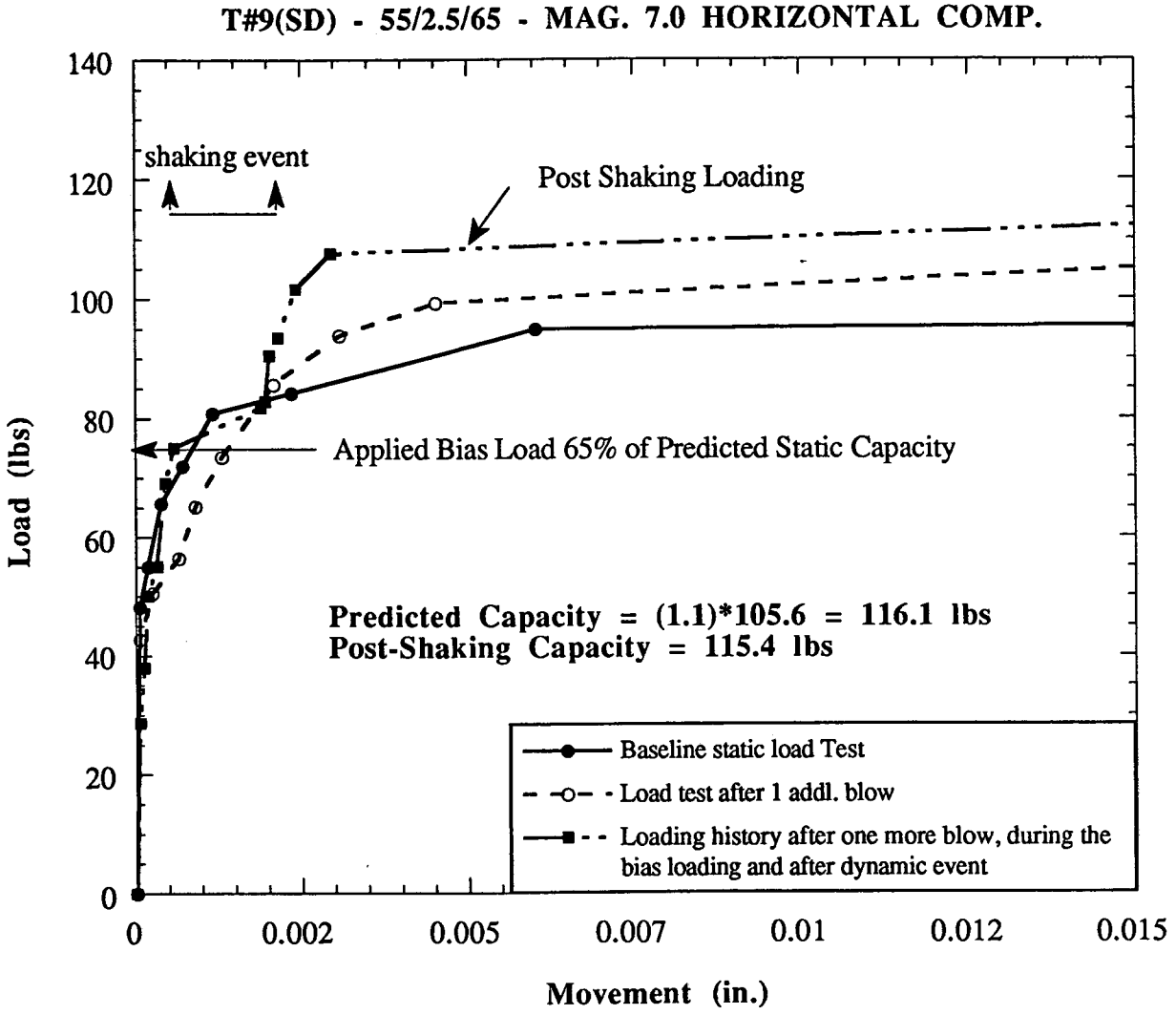

Fig. 5.0 : Loading History of the Pile Prior to and After the Dynamic Event

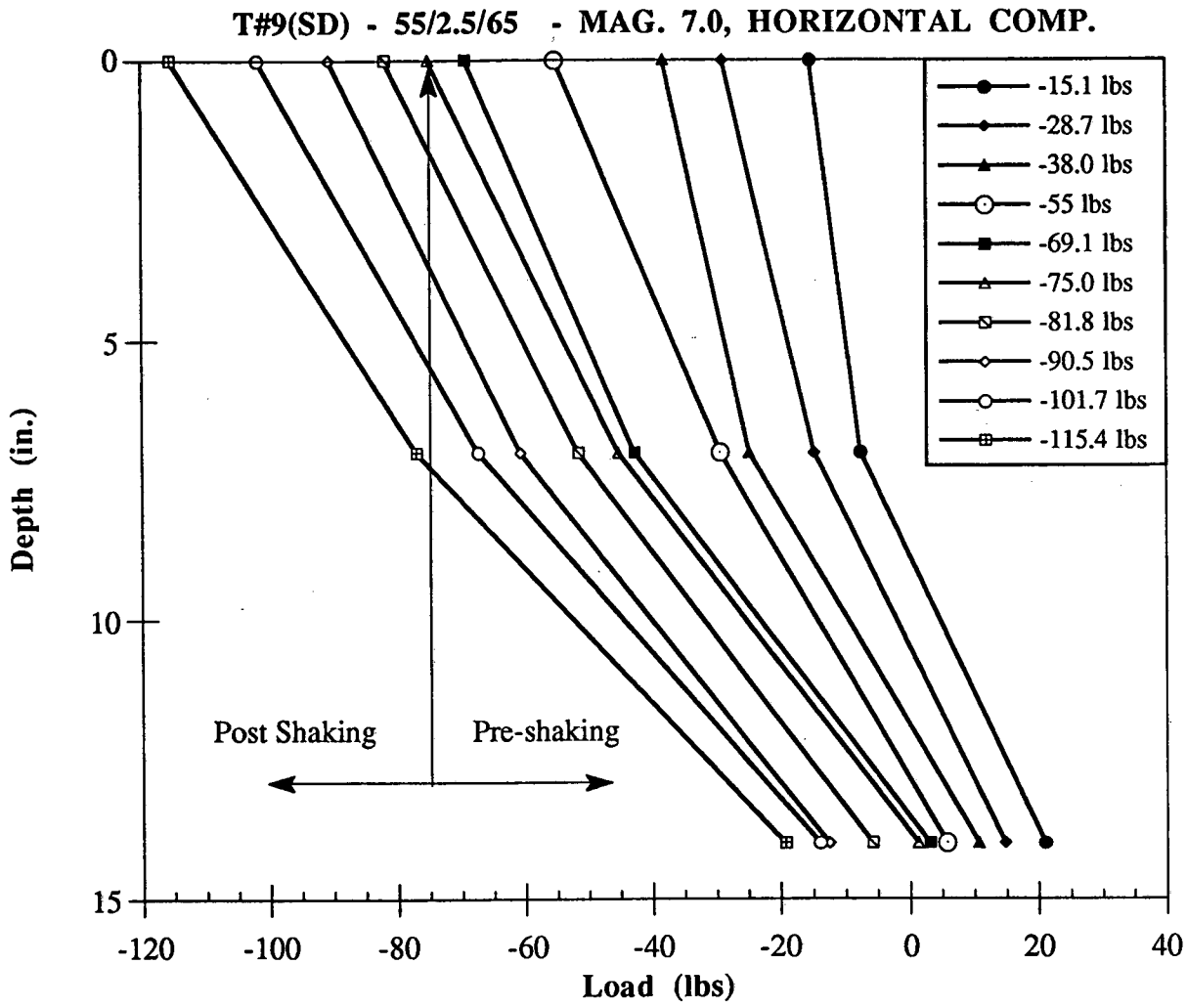

Fig. 6.0 : Load Transfer During Bias Loading And Post Shaking Test

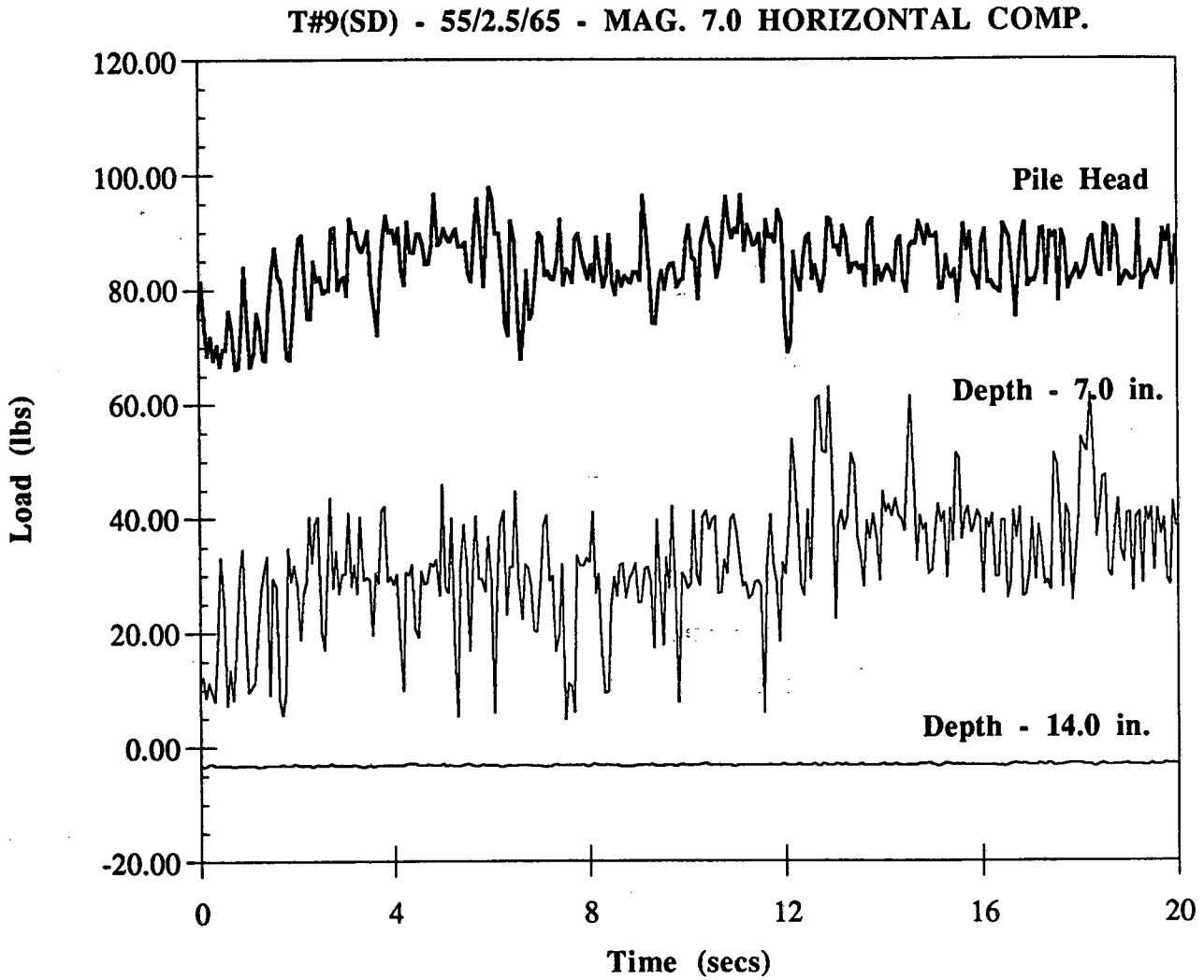

Fig. 7.0 : Loading History During the Dynamic Event

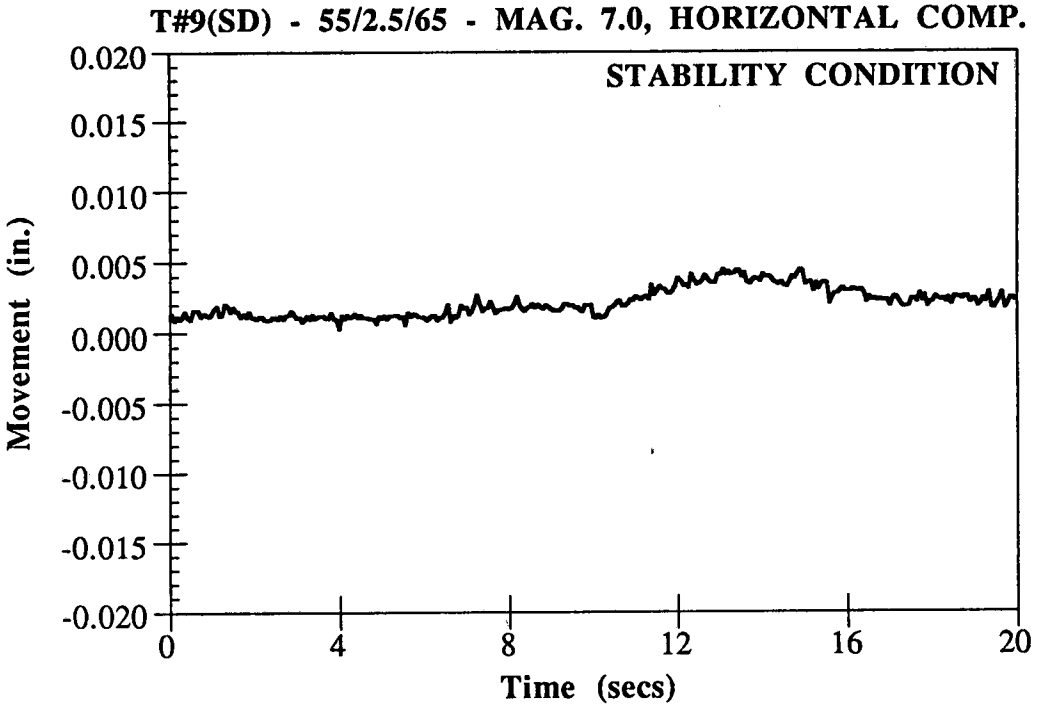

Fig. 8.0 : Pile-Head Movement Time History

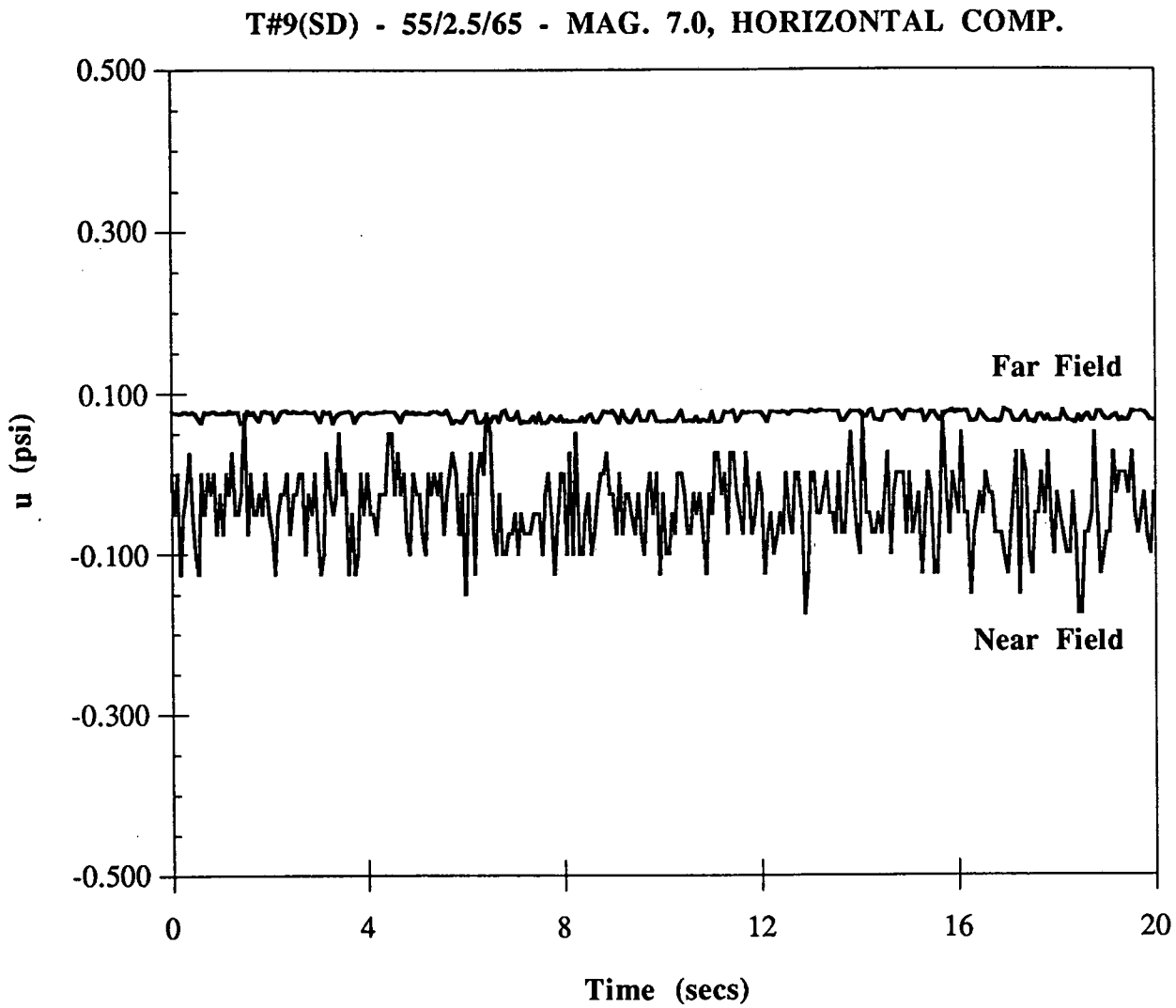

Fig. 9.0 : Pore Pressure Time History During the Dynamic Event

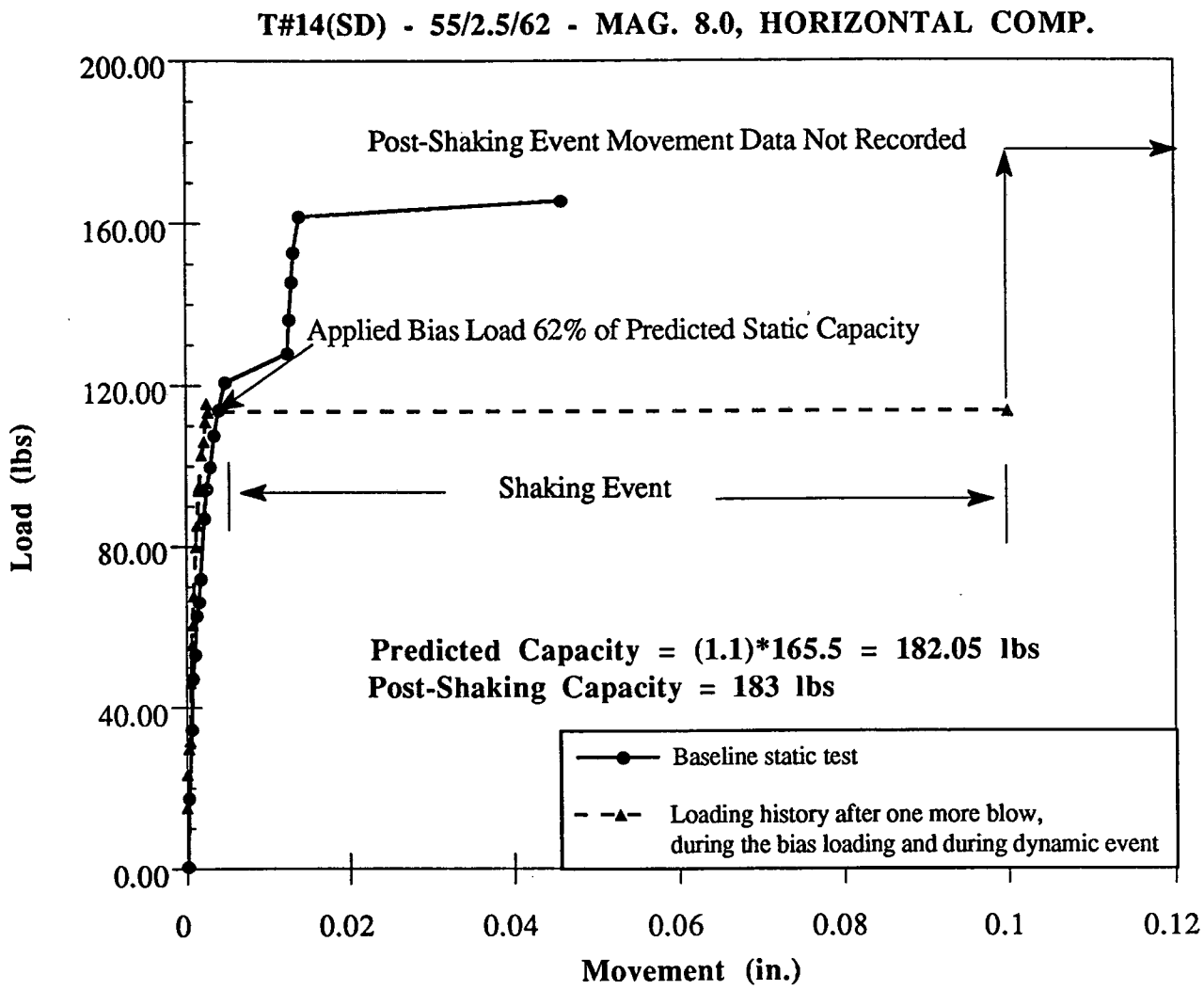

Fig. 10.0 : Loading History of the Pile Prior to and During the Dynamic Event

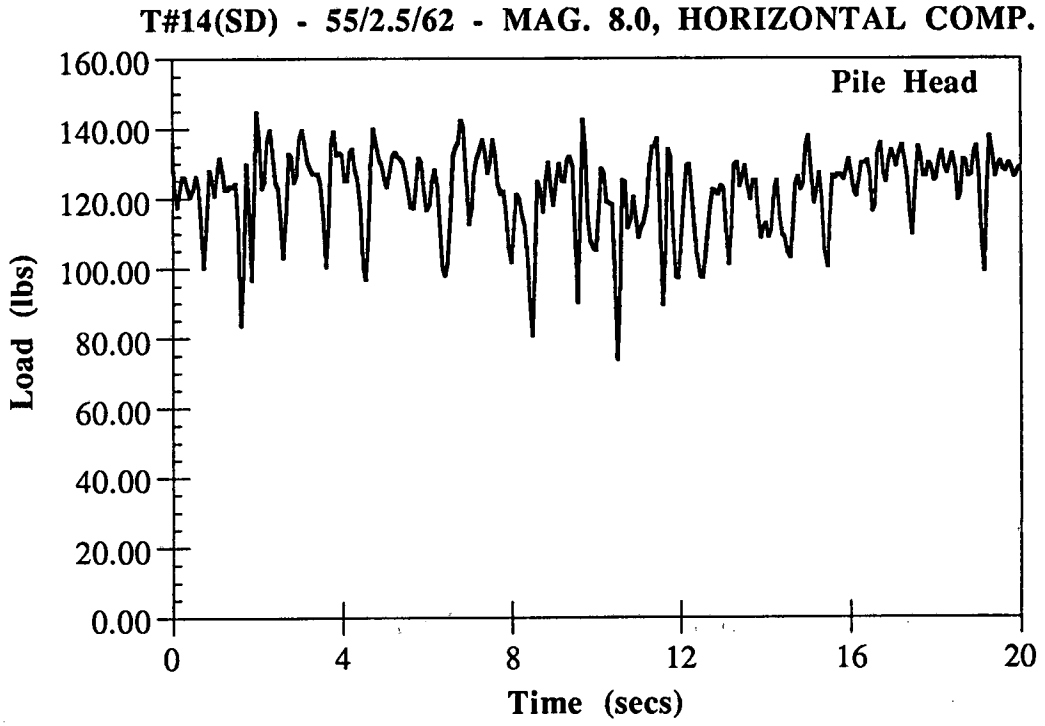

Fig. 11.0 : Loading History During the Dynamic Event

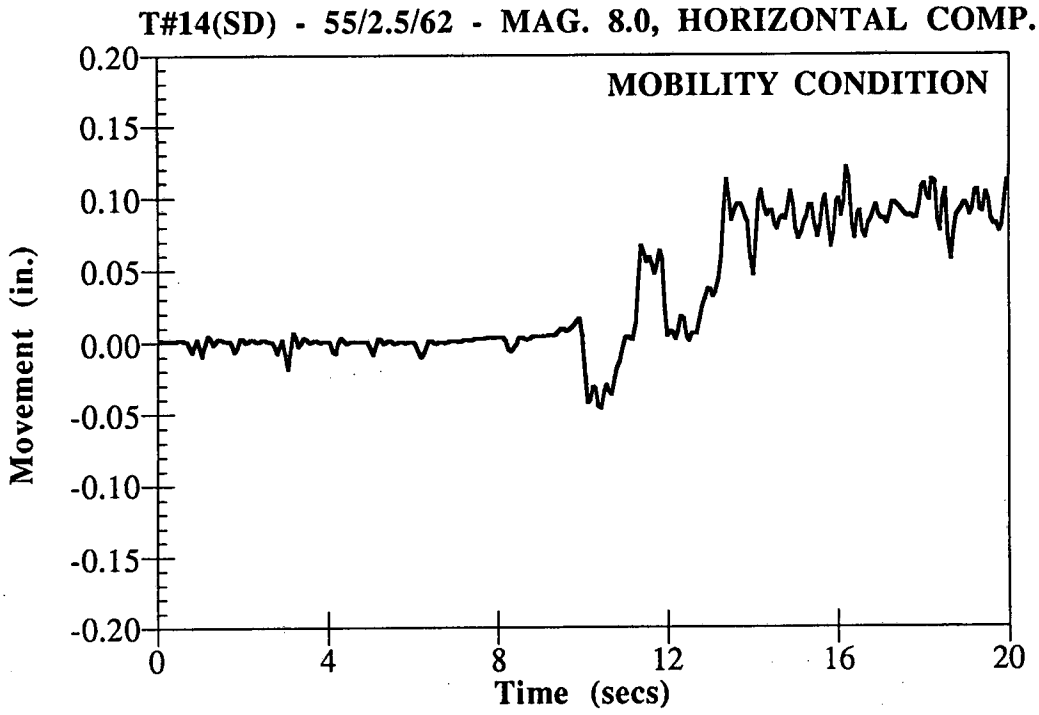

Fig. 12.0 : Pile-Head Movement Time History

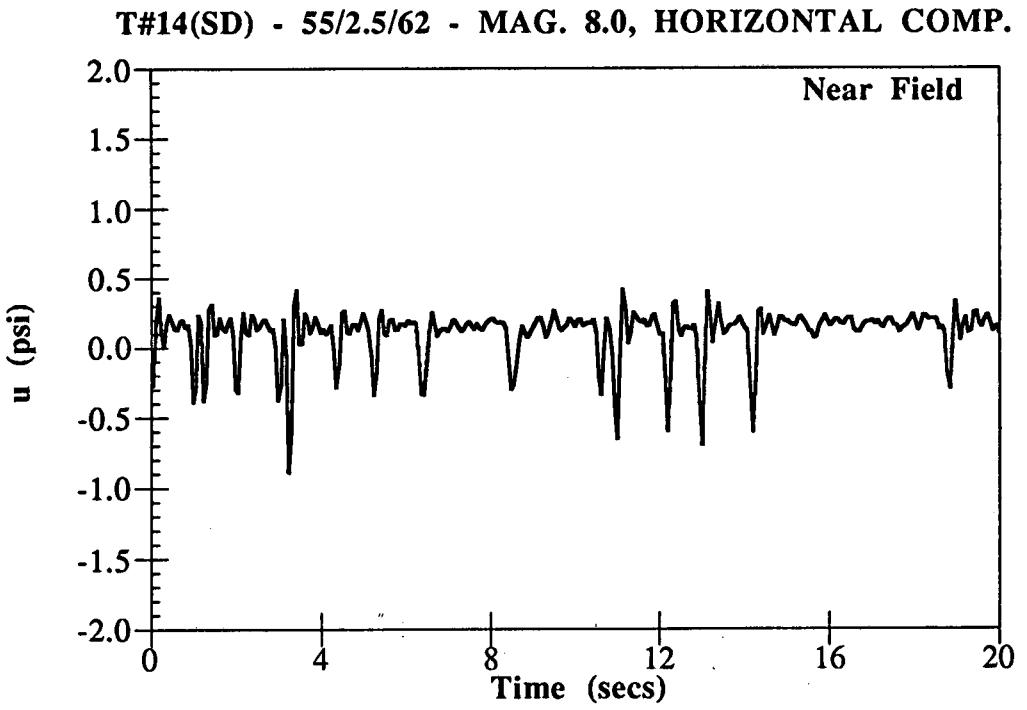

Fig. 13.0 : Pore Pressure Time History During the Dynamic Event

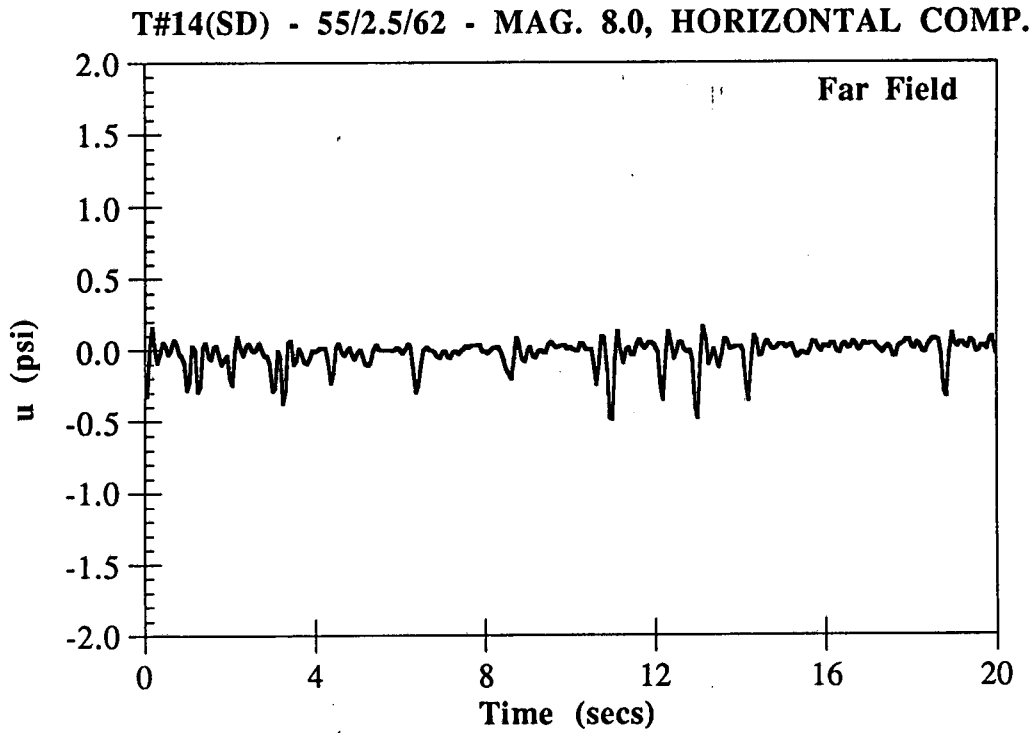

Fig. 14.0 : Pore Pressure Time History During the Dynamic Event

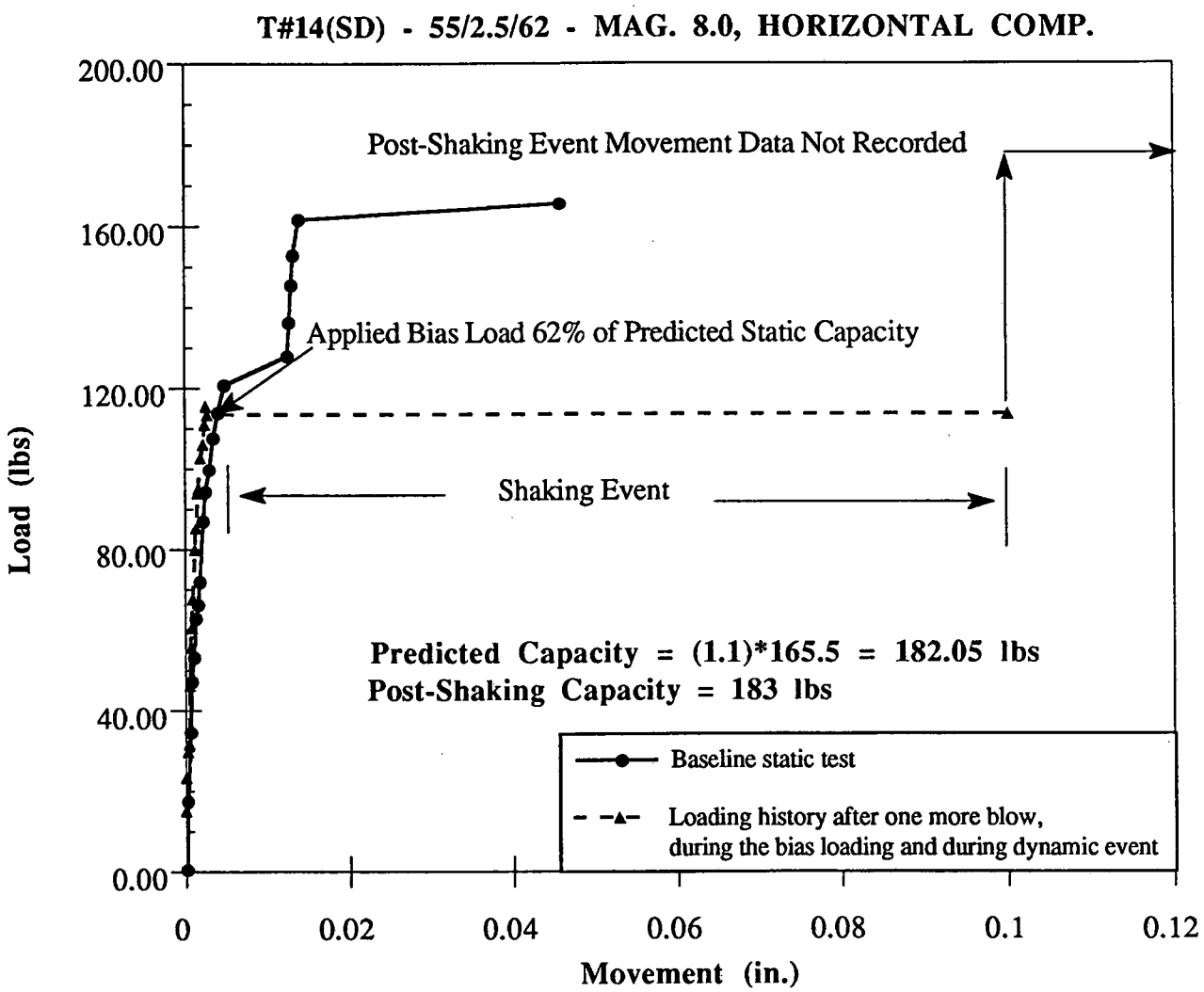

Fig. 15.0 : Loading History of the Pile Prior to and During the Dynamic Event

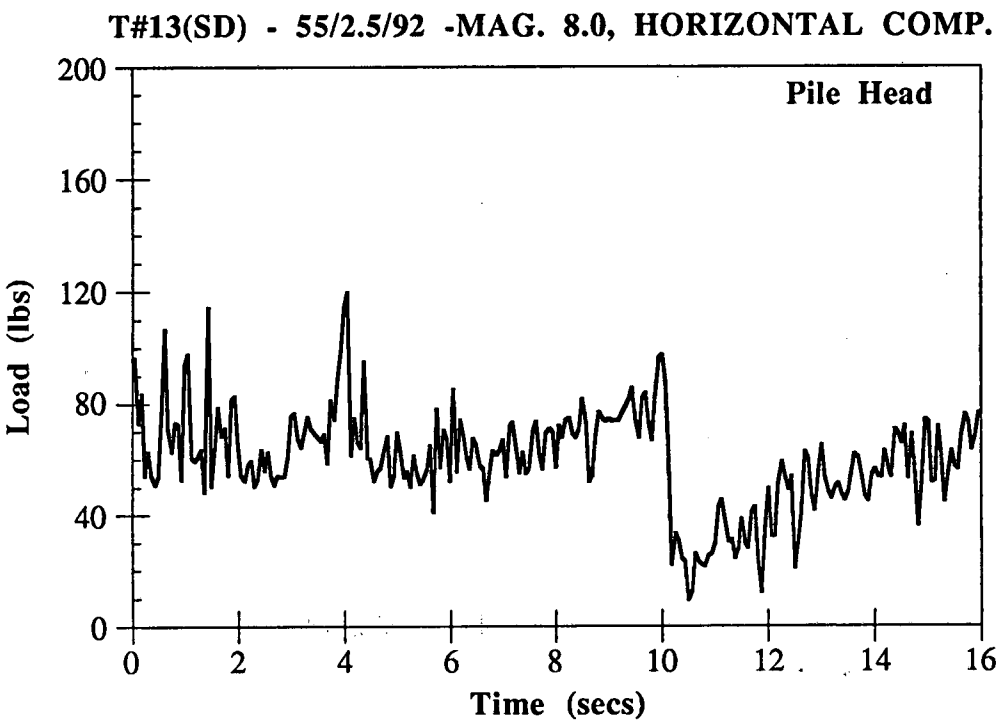

Fig. 16.0 : Loading History During the Dynamic Event

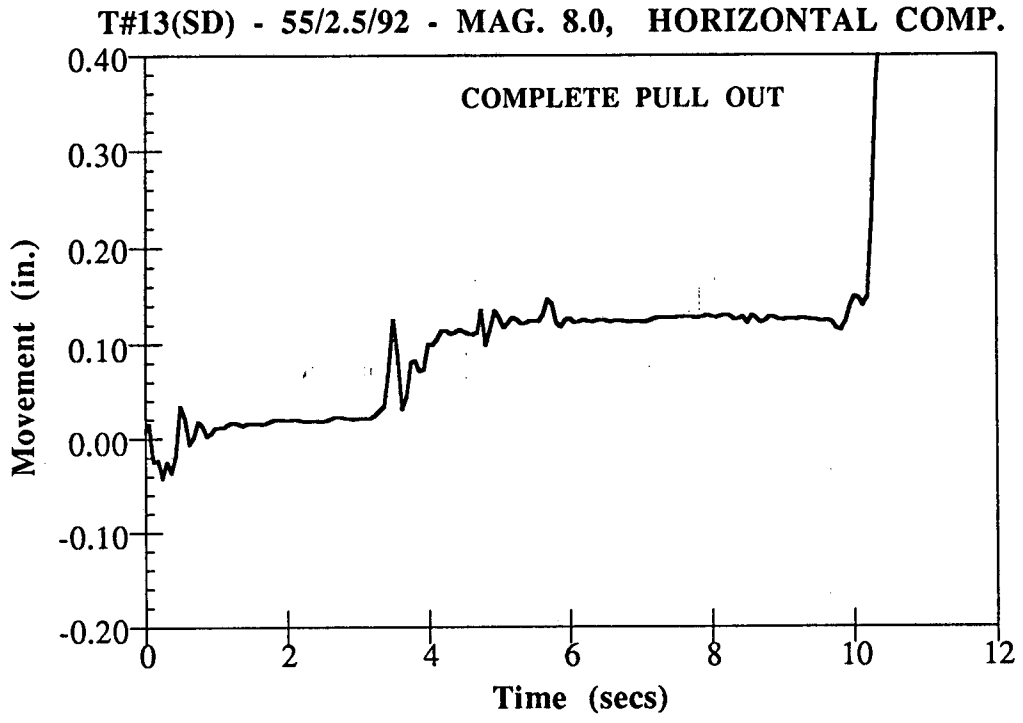

Fig. 17.0 : Pile-Head Movement Time History

59

5. For both stability and mobility condition, the post shaking capacity was 10% higher than the initial baseline static capacity. Since this value is within the scatter range of the capacity that could be expected after restrike, for all practical purposes the pile retained its static capacity subsequent to shaking.

II Signature Series :

Objective :

The objective of this study was to investigate the effect of signature of an earthquake on the pile response in terms of its effects on the contours established for stability, mobility and failure condition of the pile in the previous study with the July 13th 1986 Oceanside event.

Scaling :

1. The earthquake selected for comparison purposes was the February 28th 1990 Upland earthquake event, primarily because this earthquake had almost the same magnitude and epicentral distance from the SEMS Instrument Station as the July 13th 1986 oceanside event. Moreover, the recording stations were offshore in both cases and the duration of shaking was also about the same. Location of the epicenter for the Upland earthquake and the recording station are shown in the Fig. 18.0.

2 Both horizontal and vertical components of the acceleration records were made available. However, a study with the oceanside event suggested that the vertical component did not contribute to the pile response significantly. Initial tests were therefore conducted with the horizontal component only. The horizontal components of accelerations in the two orthogonal directions X and Y were combined together to obtain a record in the major principal variance direction. The azimuth of the X and Y directions were not available. The analytical treatment has been dealt by Penzien and Watabi (1975). The idea is to evaluate the variance and covariances of the acceleration records in the two directions and to obtain the principal variances and corresponding principal directions as the eigen values and eigen vectors respectively by solving the characteristic equation.

3 The combined x and y components of the Upland earthquake and the Oceanside event are shown in Figs 19.0 and 20.0 respectively. It can be seen that the peak acceleration in case of the Upland earthquake was about 30 milli-g whereas that in the case of the oceanside event was about 25 milli-g. The corresponding Fourier spectra for these events are shown in Fig. 21.0. Comparison of the two fourier spectra indicate that the Upland earthquake could be characterized as a low frequency earthquake as compared to the oceanside event. The predominant frequency range of the Upland event was between 0.5Hz - 2Hz with the peak at about 1 Hz whereas, the oceanside event had a frequency range of 3Hz - 5Hz with peak at about 4 Hz. The frequency distribution in the case of the Upland event was more uniform than the oceanside event.

4 The events were scaled up to magnitudes 7.0, 7.5 and 8.0. by matching the fourier amplitude spectrum of the original earthquake acceleration records to the spectrum corresponding to a higher magnitude earthquake. The fourier amplitude spectra of the original, targeted and the scaled (Mag. 7.0) earthquake record for the Upland earthquake is shown in Fig. 22.0. The scaled acceleration record for magnitude 7.0 Upland earthquake is shownn in Fig. 23.0. Similar procedure was followed for scaling to magnitudes 7.5 and 8.0 .

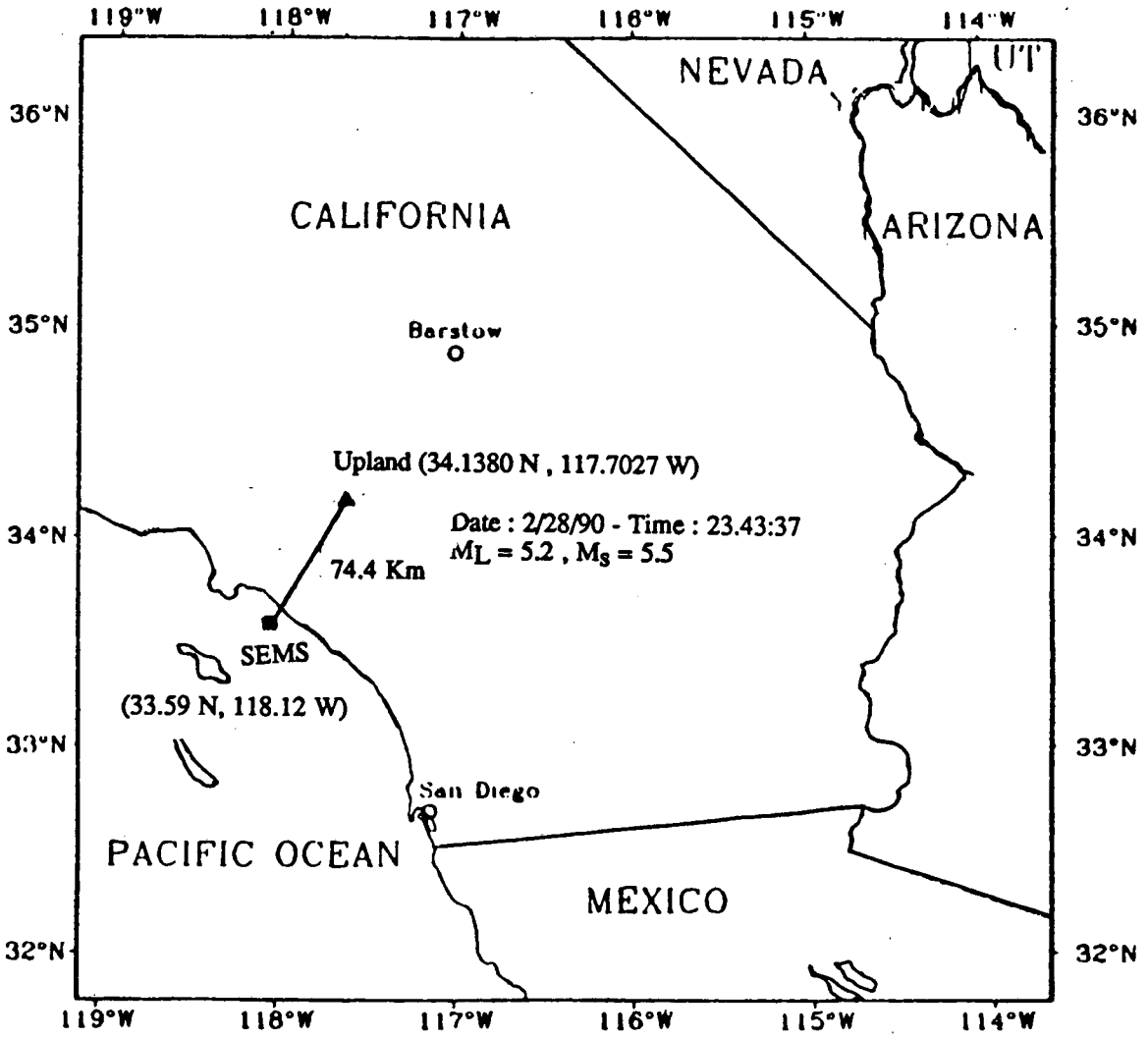

Fig. 18.0 : Map Showing Location of the Upland Earthquake Epicenter and the SEMS Instrument Station

5 The duration of significant shaking is very much influenced by the magnitude of the earthquake, because shaking is likely to continue at least as long as the fault continues to rupture. Hence the duration of strong shaking i.e. the record from 25sec - 40 sec was repeated to produce the desired duration. The extended record for the magnitude 7.0 Upland earthquake is shown in Fig. 24.0. Similar extended records were also derived for magnitudes 7.5 and 8.0.

6 The extended record for each magnitude was then integrated to obtain the desired velocity and displacement time record. The integrated time records are sensitive to the number of points selected in the integration process. Hence, the number of points for integration were selected such that the mean value of acceleration and the mean value of velocity at the end of the window were zero. A typical sensitivity study for magnitude 7.0 upland earthquake record is shown in Fig. 25.0. Figs 26.0 and 27.0 show the corresponding velocity and displacement time history records for the magnitude 7.0 upland earthquake. The displacement-time histories for the magnitude 7.5 and 8.0 upland event are also illustrated in figs 28.0 and 29.0. Both displacement and time in Figs. 27.0 , 28.0 and 29.0 were then scaled down by 5.3 to obtain the actual scaled records that were applied to the chamber.

Testing Program :

1 Dynamic Tests have been conducted with 7.0 mag. horizontal component of the Upland event in microfine sand under 2.5 psi confining pressure and 55% relative density. Initial results with bias loads in the range of 65% - 75% of the uplift capacity of the pile indicate mobility condition. However, at this point the data obtained in these tests have not been analyzed completely and hence test results are not presented here. At this point of time, tests are still in progress with 7.5 and 8.0 magnitude earthquake events and therefore zones for stability, mobility, and failure have not been established for the Upland earthquake.

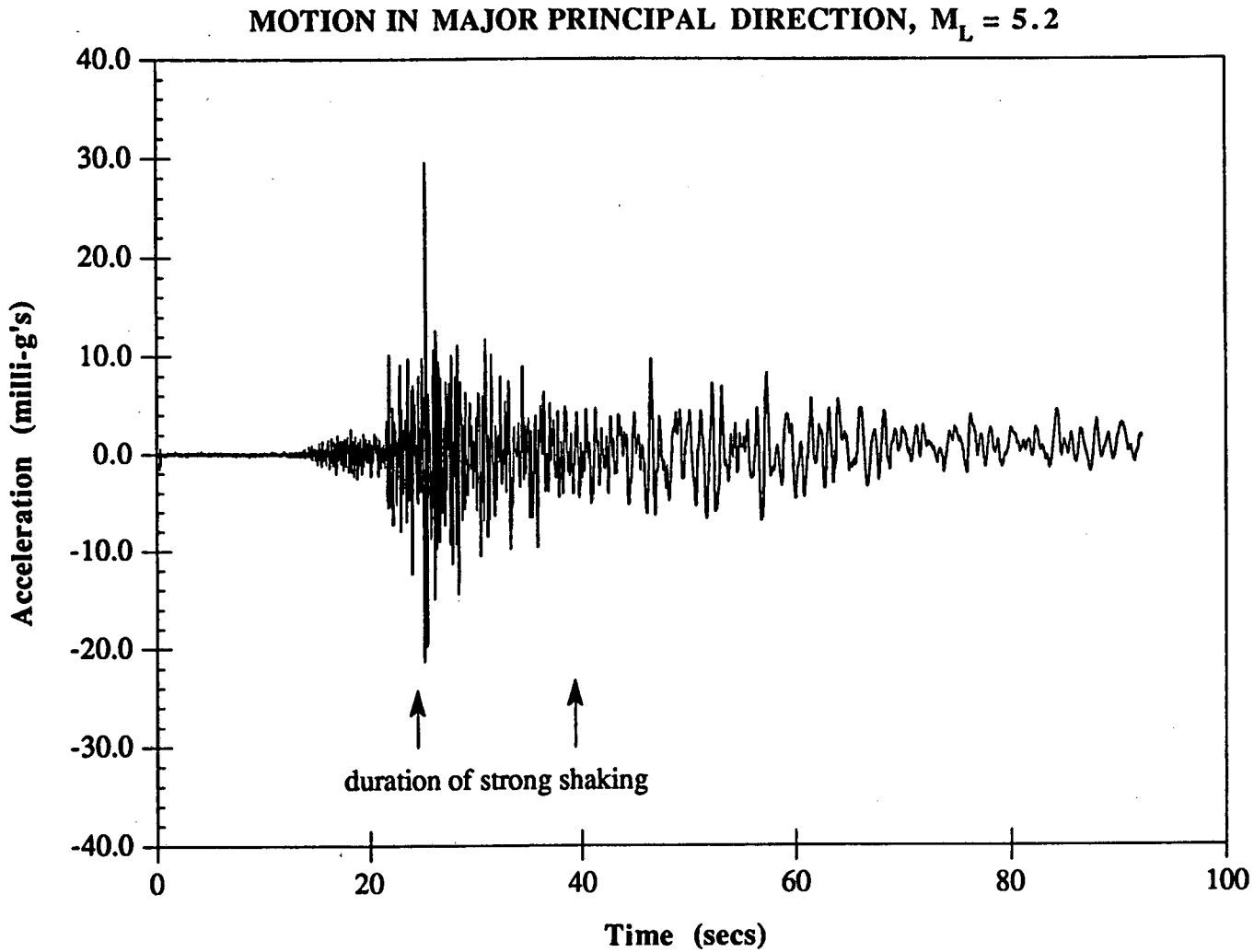

Fig. 19.0 Combined X and Y Components of Upland Earthquake (M_L = 5.2)

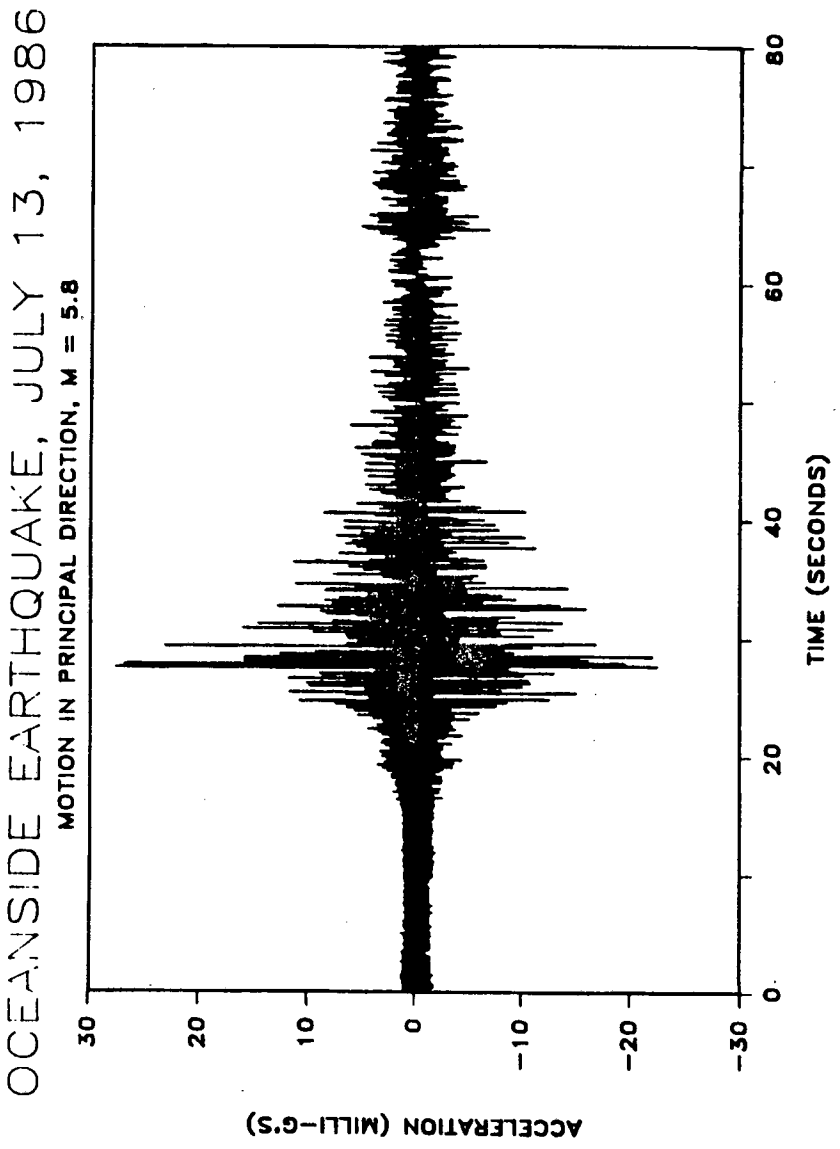

Fig. 20.0 Combined X and Y Components of Oceanside Earthquake (M=5.8).

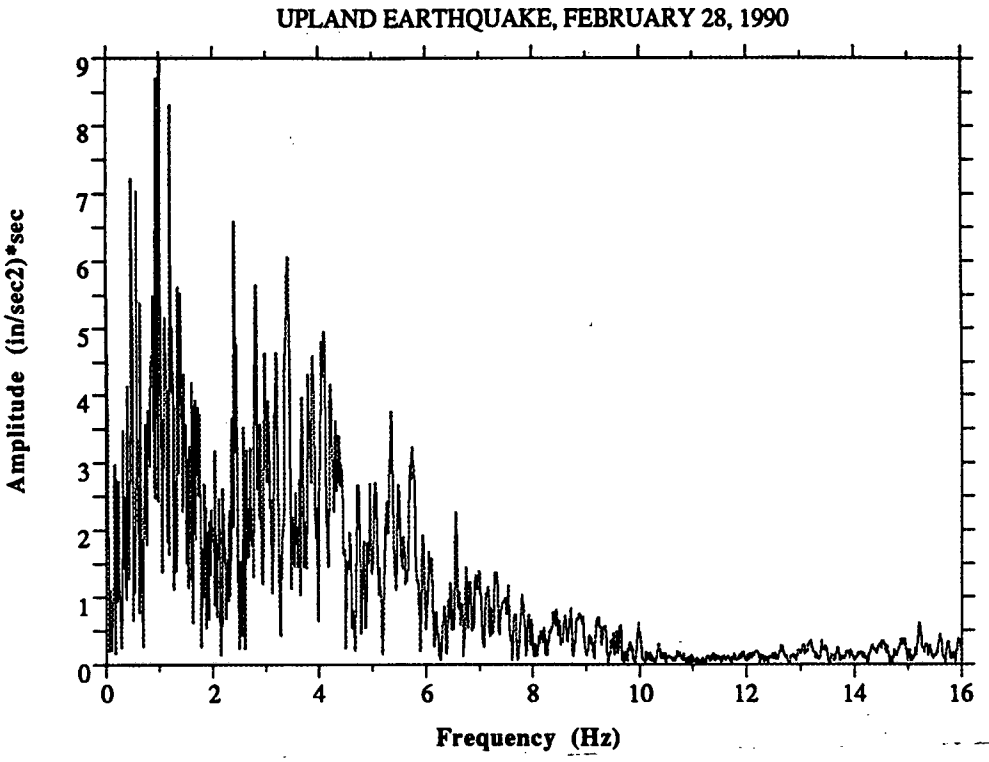

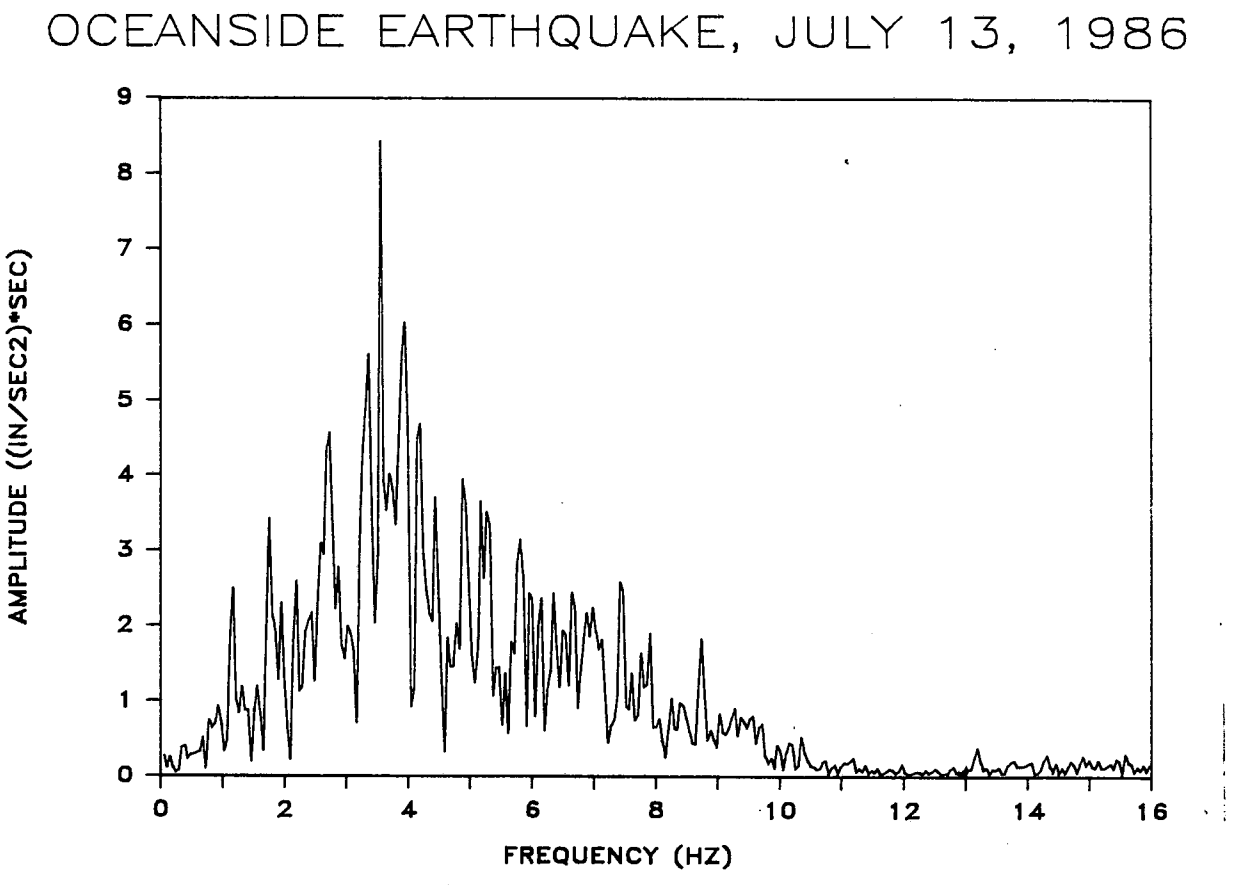

Fig. 21.0 : Fourier Amplitude Spectra of the Acceleration Record for Upland and the Oceanside event

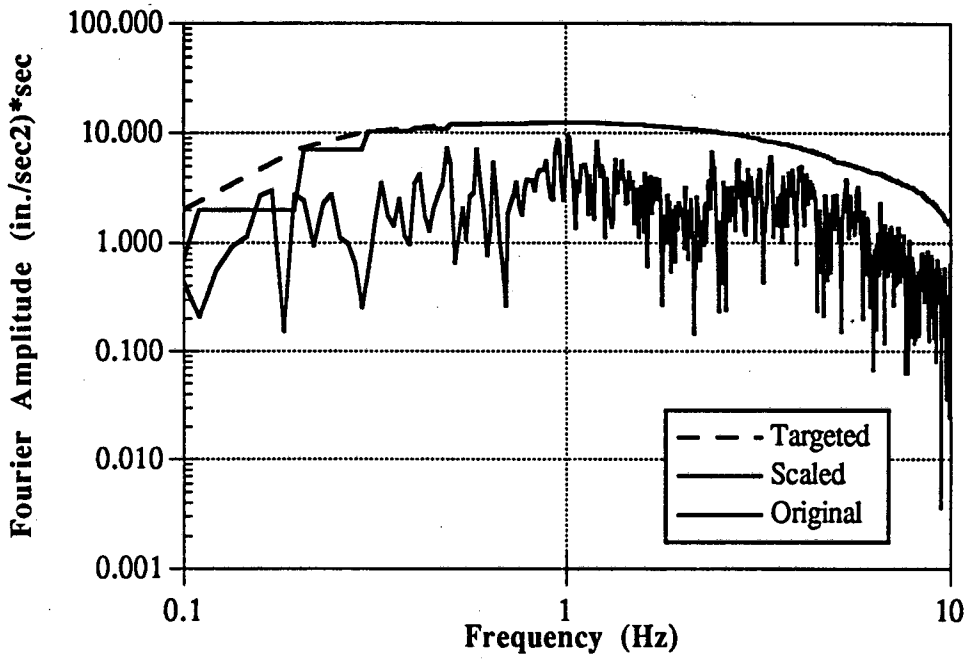

Fig. 22.0 Fourier Amplitude Spectrum (M = 7.0)- Upland Earthquake

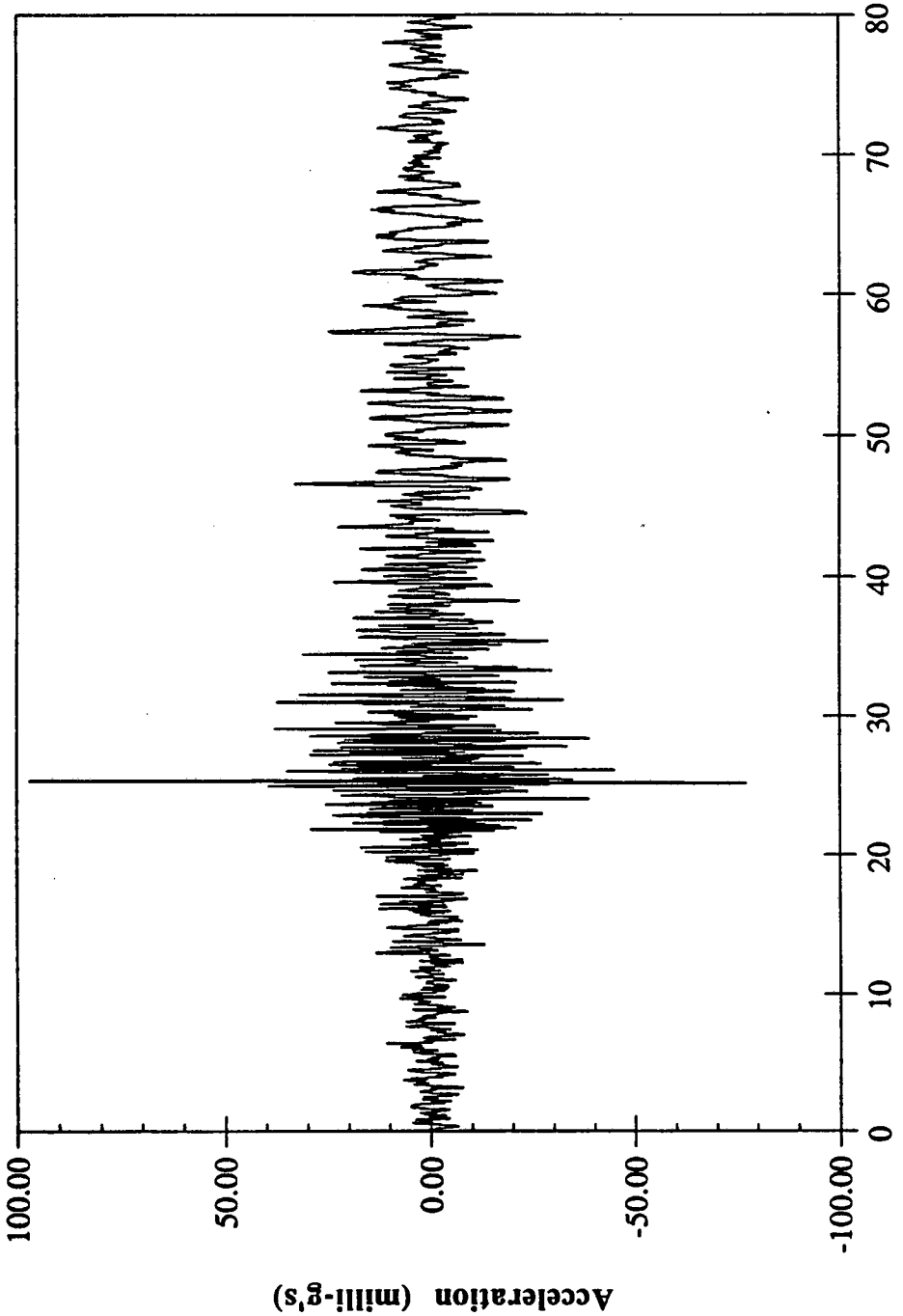

Fig. 23.0 Scaled Horizontal Comp. of the Upland Earthquake Record (Mag. 7.0)

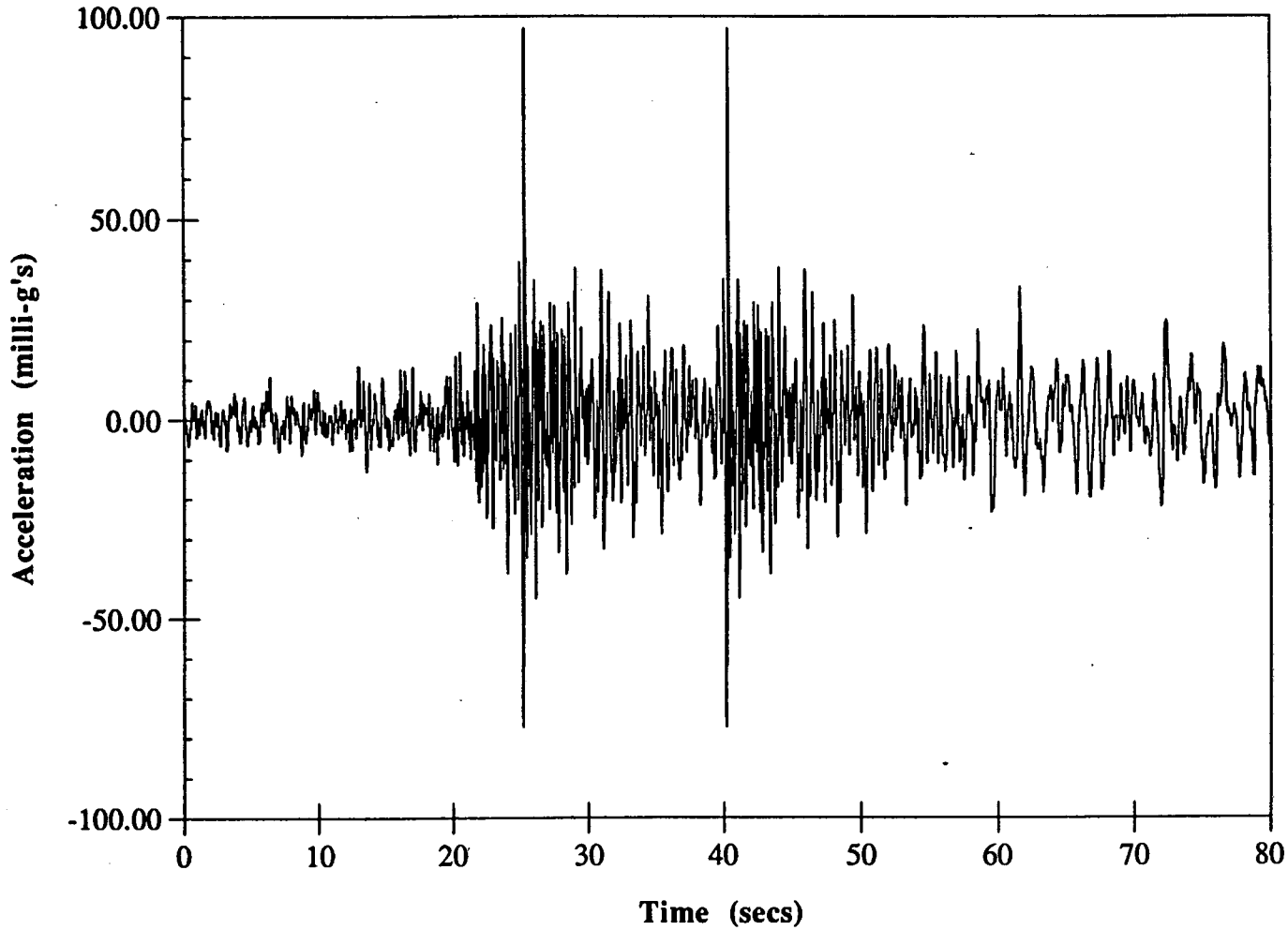

Fig. 24.0 Extended Scaled Horizontal Comp., Mag. 7.0, Upland Earthquake

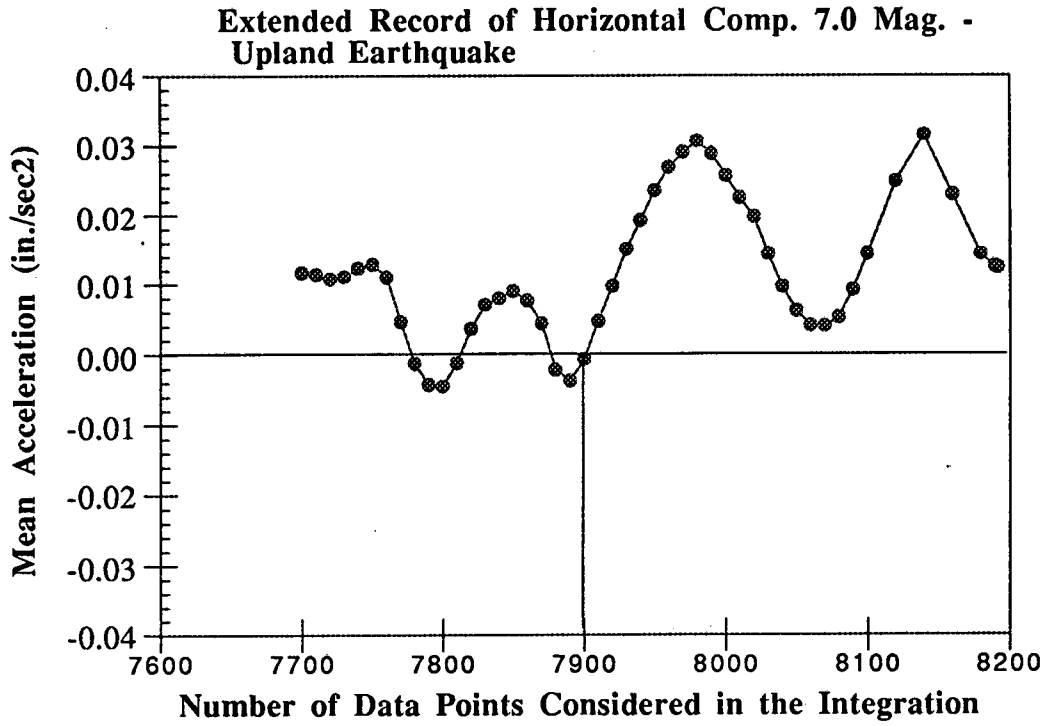

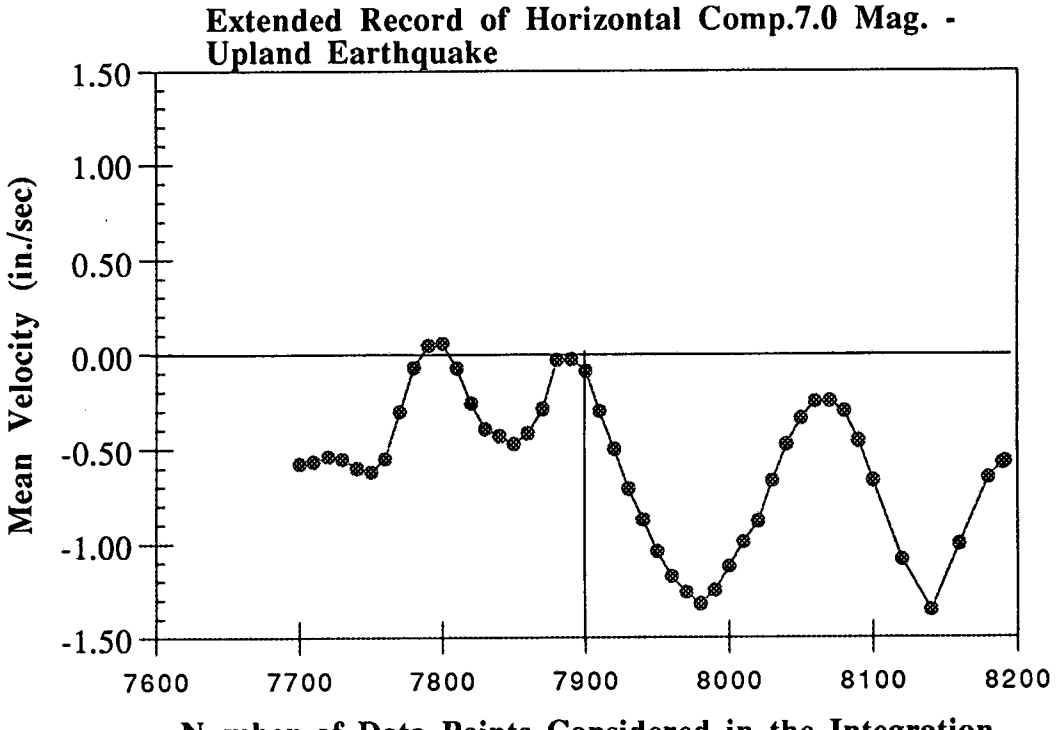

Fig. 25.0 : Selection of Number of Points for Integration

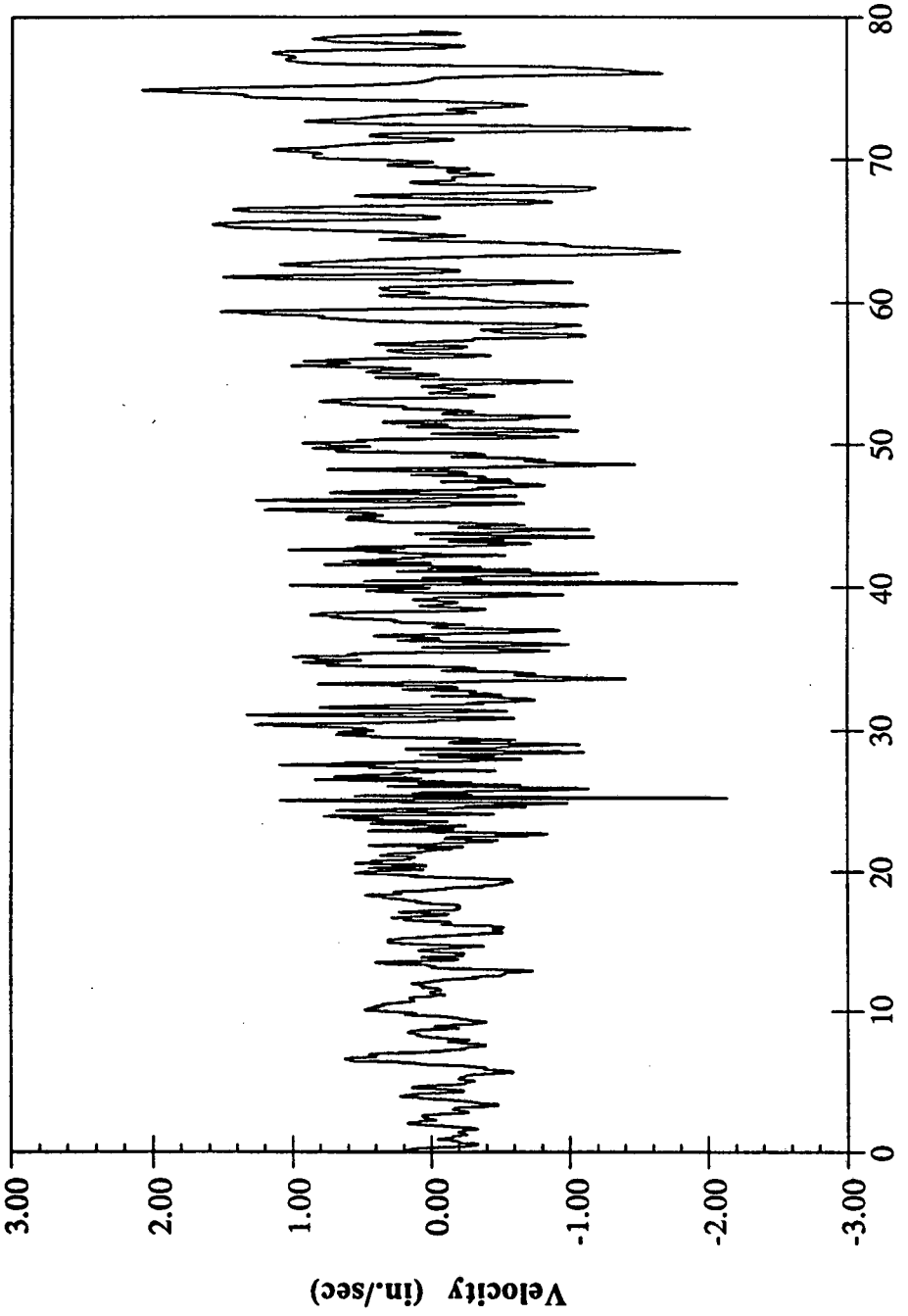

Fig. 26.0 Velocity-Time History of the Extended Record of the Upland Earthquake (Mag. 7.0)

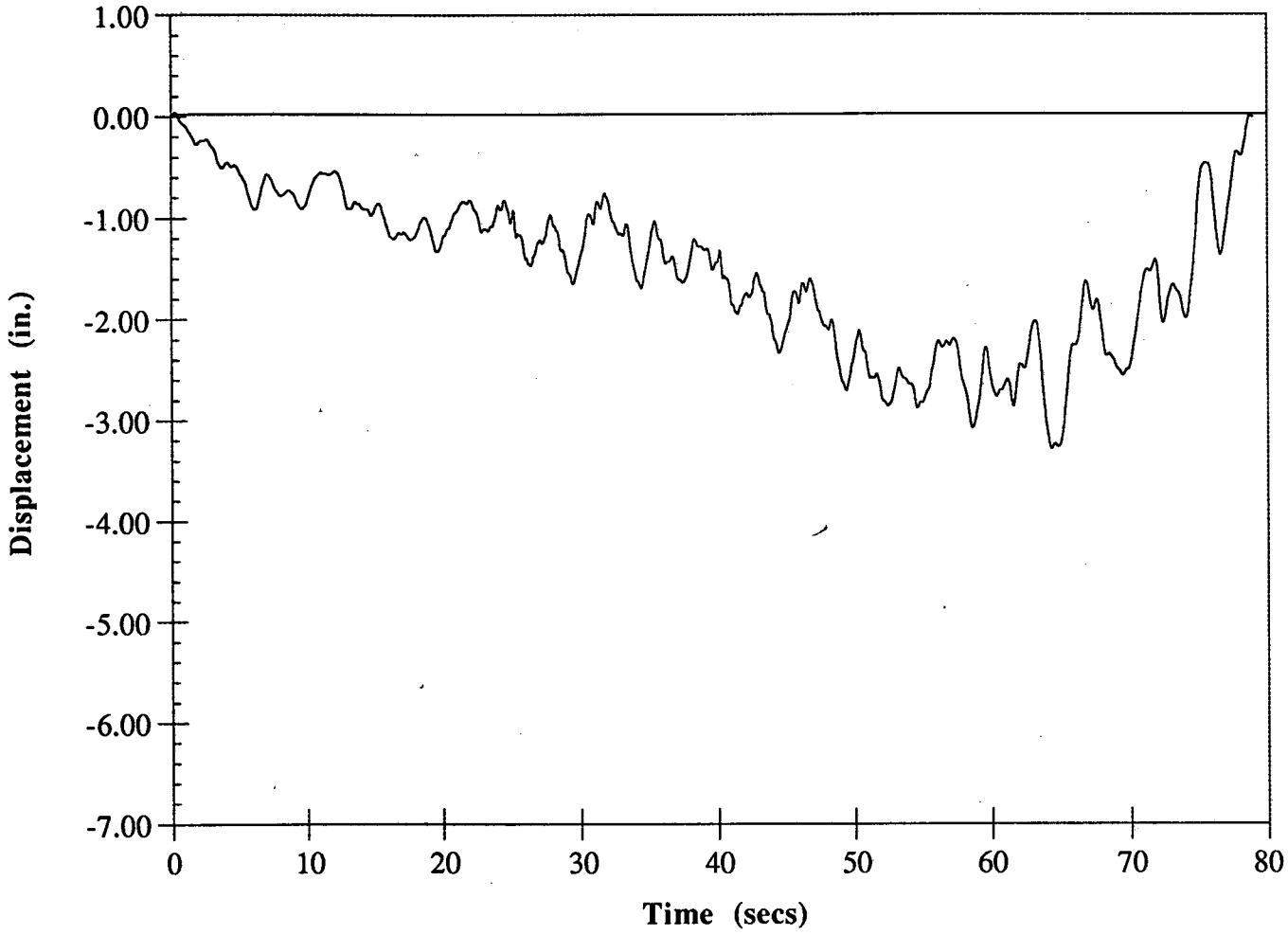

Fig. 27.0 : Displacement-Time History of the Extended Record of the Upland Earthquake (Mag. 7.0)

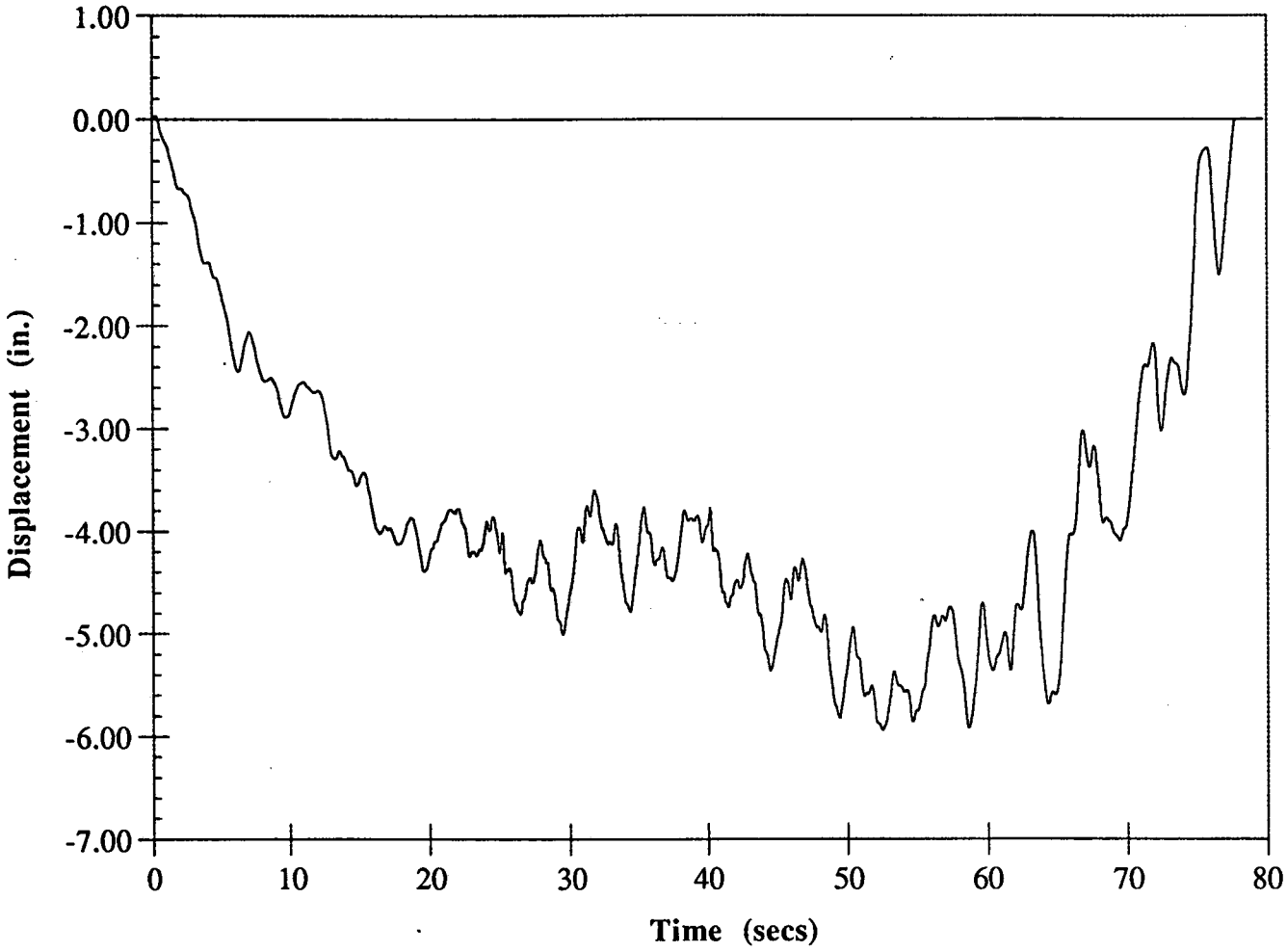

Fig. 28.0 : Displacement-Time History of the Extended Record of the Upland Earthquake (Mag. 7.5)

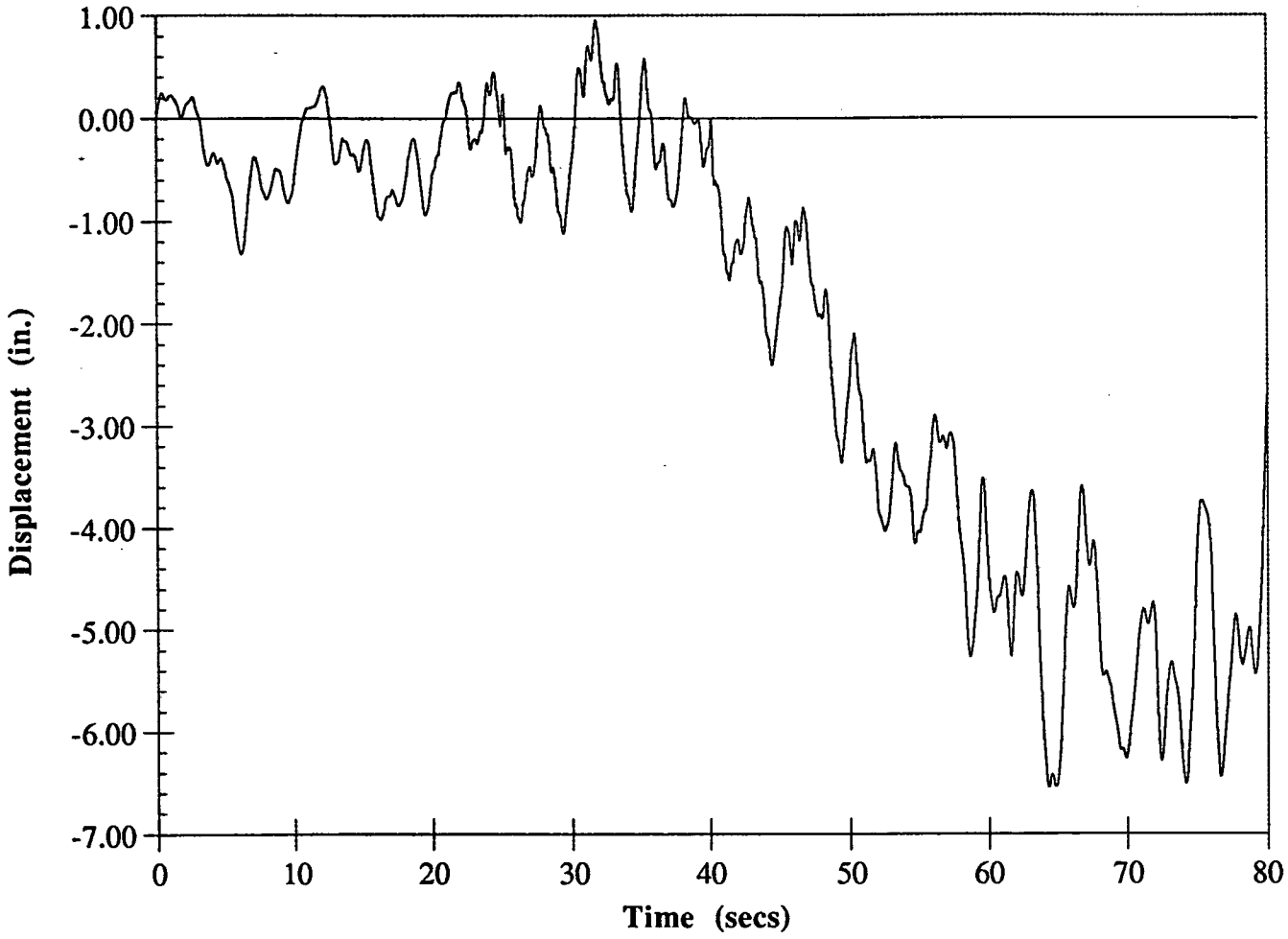

Fig. 29.0 : Displacement-Time History of the Extended Record of the Upland Earthquake (Mag. 8.0)